Global and Planetary Change 222 (2023) 104073

Contents lists available at ScienceDirect

Global and Planetary Change

journal homepage: www.elsevier.com/locate/gloplacha

Poleward amplification, seasonal rainfall and forest heterogeneity in the Miocene of the eastern USA

Tammo Reichgelt [a,*], Aly Baumgartner [b], Ran Feng [a], Debra A. Willard [c]

[a] Department of Earth Sciences, University of Connecticut, Storrs, CT, USA
[b] Sternberg Museum of Natural History, Fort Hays State University, Hays, KS, USA
[c] US Geological Survey, Reston, VA, USA

ARTICLE INFO

Editor: Dr. Alan Haywood

Keywords:
Temperature
Miocene
Paleoflora
Nearest living relative
Precipitation
North America
Proxy-model comparison

ABSTRACT

Paleoclimate reconstructions can provide a window into the environmental conditions in Earth history when atmospheric carbon dioxide concentrations were higher than today. In the eastern USA, paleoclimate reconstructions are sparse, because terrestrial sedimentary deposits are rare. Despite this, the eastern USA has the largest population and population density in North America, and understanding the effects of current and future climate change is of vital importance. Here, we provide terrestrial paleoclimate reconstructions of the eastern USA from Miocene fossil floras. Additionally, we compare proxy paleoclimate reconstructions from the warmest period in the Miocene, the Miocene Climatic Optimum (MCO), to those of an MCO Earth System Model. Reconstructed Miocene temperatures and precipitation north of 35°N are higher than modern. In contrast, south of 35°N, temperatures and precipitation are similar to today, suggesting a poleward amplification effect in eastern North America. Reconstructed Miocene rainfall seasonality was predominantly higher than modern, regardless of latitude, indicating greater variability in intra-annual moisture transport. Reconstructed climates are almost uniformly in the temperate seasonal forest biome, but heterogeneity of specific forest types is evident. Reconstructed Miocene terrestrial temperatures from the eastern USA are lower than modeled temperatures and coeval Atlantic sea surface temperatures. However, reconstructed rainfall is consistent with modeled rainfall. Our results show that during the Miocene, climate was most different from modern in the northeastern states, and may suggest a drastic reduction in the meridional temperature gradient along the North American east coast compared to today.

1. Introduction

The Miocene spans 23.03 to 5.33 million years ago (Walker et al., 2018) and witnessed the major temperature decline into the Quaternary icehouse (Pound et al., 2012; Herbert et al., 2016; Super et al., 2018) and a reduction in global atmospheric CO_2 (Super et al., 2018; Witkowski et al., 2018; Steinthorsdottir et al., 2021. Though proxy reconstructions of Miocene atmospheric CO_2 are debated (Kürschner et al., 2008; Sosdian et al., 2018; Super et al., 2018; Witkowski et al., 2018; Reichgelt et al., 2020), it is likely that modern atmospheric CO_2 has already surpassed that of the Messinian – Tortonian (~400 ppm) and the Earth's atmosphere will be reaching atmospheric CO_2 similar to the Serravallian and Langhian (>500 ppm) over the next few decades (e.g., Prentice et al., 2001; Foster et al., 2017). As such, Miocene climate can serve as a near-future model of global and regional climate conditions.

Using the Mississippi River as the western boundary, the eastern United States is home to >50% of the country's population, at ~180 million people. Some of the projected consequences of increased atmospheric CO_2 in the eastern United States are higher average temperatures, more extreme rainfall events, an increase of temperature extremes and shifts in ecosystems (Iverson et al., 2008; Carter et al., 2018; Dupigny-Giroux et al., 2018). These projections are primarily based on climate models, but terrestrial paleoclimate studies can offer insight into climate conditions at times when CO_2 levels were higher than pre-industrial and terrestrial ecosystems had evolved in adaptation to these conditions. However, Miocene terrestrial paleoclimate reconstructions from eastern North America are sparse, in large part due to a dearth of fossiliferous strata of this age (Isphording, 1970). By contrast, abundant Miocene terrestrial fossiliferous strata from western North America revealed a major vegetation transition from C_3

* Corresponding author.
E-mail address: tammo.reichgelt@uconn.edu (T. Reichgelt).

https://doi.org/10.1016/j.gloplacha.2023.104073
Received 14 July 2022; Received in revised form 31 January 2023; Accepted 16 February 2023
Available online 20 February 2023

vegetation to C_4 grassland (Janis et al., 2004; McInerney et al., 2011). With continuous C_3 dominance, a Miocene forest to grassland transition is absent from eastern North America (Pazzaglia et al., 1997; Shunk et al., 2006; Kotthoff et al., 2014; Prader et al., 2017), but it is unclear whether forests were heterogenous through space and time.

Though Miocene terrestrial sediments containing fossil plants are sparse in eastern North America, several microfloral studies from marine (Frederiksen, 1984; Brenner et al., 1997; Groot, 1998; Weems et al., 2017) and terrestrial depositional settings (Rachele, 1976; Pazzaglia et al., 1997; Rich et al., 2002) and megafloral localities (Berry, 1916; McCartan et al., 1990; Farlow et al., 2001; Gong et al., 2010; Jarzen et al., 2010; Liu and Jacques, 2010; Tiffney et al., 2018; Lott et al., 2019; McNair et al., 2019; Swinehart and Farlow, 2021) are known. These records span the Aquitanian to the Messinian (23.03 to 5.33 Ma), but have a scattered distribution from Florida to Vermont (Table 1). Fossil plants preserve a snapshot of Earth's climatic history because plant physiognomy and distribution are limited by their abiotic environment, and modern climatic relationships to plant physiognomy or distribution can thereby be used to reconstruct terrestrial paleoclimate (e.g., Utescher et al., 2014; Peppe et al., 2018; Spicer et al., 2020).

In this study, we explore Miocene terrestrial paleoclimate and vegetation through previously collected and published paleofloras from the eastern USA (Table 1). The main goal is to use consistent paleoclimate and paleoecology reconstruction techniques on all paleofloras in order to compare spatial and temporal Miocene trends in terrestrial climate and vegetation. We compare the terrestrial paleoclimate reconstructions with those from the marine realm and to a new mid-Miocene climate simulation. Finally, we explore the closest representative modern vegetation types of the Miocene fossil floras and assess whether the eastern USA witnessed Miocene forest changes.

2. Materials and methods

2.1. Eastern USA Miocene paleofloras

Miocene paleofloras in the eastern USA are scattered across numerous states (Fig. 1). The sites included in this study represent previously documented Miocene floras that reported 1) full floral assemblages, and 2) age constraints. We provide ages of the floras as they were reported in their respective studies (Table 1). Palynofloral records from marine sediments of the New Jersey coastal plain provide semi-continuous records through parts of the Miocene, including the Calvert, Choptank, St Marys and Eastover Formations (Brenner et al., 1997; Weems et al., 2017; Fig. 2). In this study, palynofloral records from four

Table 1
Summary of paleofloral sites from the eastern USA used in this study, including modern (Mod) and Miocene (Mio) coordinates (Müller et al., 2018). Aqu = Aquitanian Bur = Burdigalian, Lan = Langhian, Ser = Serravallian, Tor = Tortonian, Mes = Messinian, Zan = Zanclean, Bio = biostratigraphy, Lith = lithostratigraphy, pal = palynology, vert = vertebrates, rad = radiolarians, for = foraminifera.

Site name	Fossil provenance	Loc (°N, °E) Mod – Mio	Age range (MYA)	Dating method	Formation
Brandon Lignite[1,2,3] (VT)	Macro- & microfossils	43.82, −73.06 42.47, −68.13	18–20 (Bur)	Bio (pal)[2]	NA
Legler Lignite[4,5] (NJ)	Local & regional microfossils	40.03, −74.33 39.22, −71.82	10–12 (Ser/Tor)	Lith[5]	Cohansey
Alum Bluff[6,7] (FL)	Macro- & microfossils	30.47, −84.99 29.8, −81.47	13.6–16 (Lan)	Bio (vert)[7]	Fort Preston
Pollack Farm[8] (DE)	Local & regional microfossils	39.2, −75.6 38.02, −71.18	17.3–19.2 (Bur)	Bio (rad)[28], $^{87}Sr/^{86}Sr$[29]	Calvert
Belvidere[9] (MD)	Regional microfossils	39.6, −76.01 38.84, −73.57	5.3–16 (Lan – Mes)	Bio (pal)[9]	Bryn Mawr
Big Creek & Chalk Hills[10,11] (LA)	Macro- & microfossils	31.8, −91.7 31.51, −89.87	8.7 (Tor)	Bio (pal & for)[11]	Catahoula
Ohoopee River[12] (GA)	Local & regional microfossils	32.7, −82.4 32.2, −80.59	3.6–13.8 (Zan – Ser)	Bio (pal)[12]	NA
Brandywine[13] (MD)	Macro- & microfossils	38.7, −76.9 38.07, −74.89	6.5–11.2 (Tor/Mes)	Bio (pal)[13]	Brandywine
Gray Fossil Site[14–21] (TN)	Macro- & microfossils	36.37, −82.5 36.11, −81.45	4.5–4.9 (Zan)	Bio (vert)[30]	NA
Pipe Creek[22,23] (IN)	Macrofossils	40.45, −85.79 40.2, −84.49	3.6–7.2 (Mes/Zan)	Bio (vert)[22]	NA
Stratford Hall[24] (VA)	Regional microfossils (offshore)	38.16, −76.83 37.33, −73.92	11.6–13.8 (Ser)	Bio (pal)[24]	Choptank
Stratford Hall[24] (VA)	Regional microfossils (offshore)	38.16, −76.83 37.49, −74.73	7.2–11.6 (Tor)	Bio (pal)[24]	St Marys
Stratford Hall[24] (VA)	Regional microfossils (offshore)	38.16, −76.83 37.22, −73.34	13.6–16 (Lan)	Bio (pal)[24]	Calvert
Bouie River[25] (MS)	Macrofossils	31.35, −89.31 30.93, −86.62	11.6–13.8 (Ser)	Lith, Bio (vert)[25]	Hattiesburg
Atlantic City[26] (NJ)	Regional microfossils (offshore)	39.4, −74.45 37.92, −69.15	20.4–23 (Aqu)	Bio (pal)[26]	NA
Atlantic City[26] (NJ)	Regional microfossils (offshore)	39.4, −74.45 38.17, −70.06	16–20.4 (Bur)	Bio (pal)[26]	NA
Atlantic City[26] (NJ)	Regional microfossils (offshore)	39.4, −74.45 38.37, −70.93	13.6–16 (Lan)	Bio (pal)[26]	NA
Atlantic City[26] (NJ)	Regional microfossils (offshore)	39.4, −74.45 38.5, −71.51	11.6–13.8 (Ser)	Bio (pal)[26]	NA
Marshfield[27] (MA)	Local & regional microfossils	42.11, −70.7 41.02, −67.38	11.6–16 (Lan/Ser)	Bio (pal)[27]	NA

1: Tiffney (1994), 2: Traverse (1994), 3: Tiffney and Mancher (2018), 4: Rachele (1976), 5: Greller and Rachele (1983), 6: Jarzen et al. (2010), 7: Lott et al. (2019), 8: Groot (1998), 9: Pazzaglia et al. (1997), 10: Berry (1916), 11: Wrenn et al. (2003), 12: Rich et al. (2002), 13: McCartan et al. (1990), 14: Wallace and Wang (2004), 15: Gong et al. (2010), 16: Liu and Jacques (2010), 17: Ochoa et al. (2012), 18: Huang et al. (2014), 19: Huang et al. (2015), 20: Hermsen (2021), 21: Quirk and Hermsen (2021), 22: Farlow et al. (2001), 23: Swinehart and Farlow (2021), 24: Weems et al. (2017), 25: McNair et al. (2019), 26: Brenner et al. (1997), 27: Frederiksen (1984), 28: Benson (1998), 29: Jones et al. (1998), 30: Samuels et al. (2018).

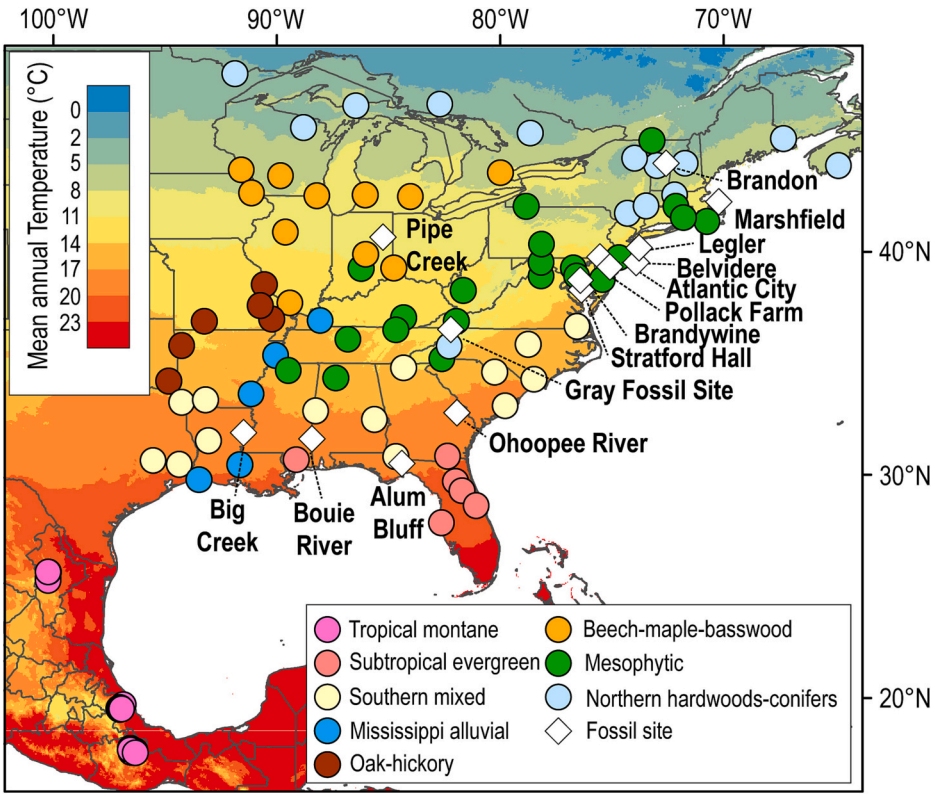

Fig. 1. Map of the eastern USA and Mexico, showing locations of fossil floras and modern vegetation sites, with vegetation types (sensu Dyer, 2006) used in determining vegetation similarities. Modern mean annual temperatures derived from Hijmans et al. (2017).

coastal plain marine deposits were included (Table 1): the Atlantic City borehole spanning the Aquitanian to Serravallian in southern New Jersey (Brenner et al., 1997), the Burdigalian Pollack Farm site in Delaware (Groot, 1998), the Middle Miocene Marshfield borehole in eastern Massachusetts (Frederiksen, 1984), and the Stratford Hall outcrops spanning the Langhian to Tortonian in northeast Virginia (Weems et al., 2017).

Several analyzed palynofloras were deposited in onshore environments (Table 1). This makes it more likely to include elements of local vegetation, rather than in marine deposits which mainly contain elements of wind-blown hinterland vegetation that tend to contribute more to pollen rain (e.g., Chevalier et al., 2020). Palynofloras deposited in onshore environments include the Middle to Late Miocene fluvial deposits of the Bryn Mawr Formation near Belvidere, Maryland (Pazzaglia et al., 1997), the Serravallian to Tortonian Legler Lignite deposit of the Cohansey Formation in New Jersey (Rachele, 1976; Greller and Rachele, 1983) and the Serravallian to Zanclean fluvial/paludal deposits at the Ohoopee River dunefield in eastern Georgia (Rich et al., 2002).

Finally, several sites have extensive taxonomically assigned megafloras associated with them, in certain cases in addition to palynofloras (Table 1). This includes the northern- and southernmost floras considered here, as well as the westernmost (Fig. 1). Megafloras are far more likely to represent local vegetation than palynofloras (e.g., Ferguson, 1985; Spicer, 1989). For this study, we analyzed floras of the Burdigalian Brandon Lignite in Vermont (Tiffney, 1994; Traverse, 1994; Tiffney et al., 2018), the Langhian Alum Bluff deposit from the Fort Preston Formation in northern Florida (Jarzen et al., 2010; Lott et al., 2019), the Serravallian Bouie River deposit of the Hattiesburg Formation in southern Mississippi (McNair et al., 2019), the Tortonian Big Creek and Chalk Hills deposit of the Catahoula Formation in Louisiana (Berry, 1916; Wrenn et al., 2003), the Tortonian to Messinian Brandywine flora in the Brandywine Formation in Maryland (McCartan et al., 1990) and the Messinian to Zanclean Pipe Creek deposit in Indiana (Farlow et al., 2001; Swinehart and Farlow, 2021). Of these sites, only the Bouie River and Pipe Creek deposits do not have associated microfloras. The Gray Fossil site in eastern Tennessee was included in our analysis too, though it has been placed in the Zanclean using biozonation (4.5–4.9 Ma, Samuels et al., 2018). It was formerly considered Messinian to Zanclean (Wallace and Wang, 2004) and because of the importance of the Gray Fossil site to our understanding of North American biotic evolution (e.g., Wallace and Wang, 2004; Huang et al., 2014, 2015; Samuels et al., 2018; Quirk and Hermsen, 2021), it is still included in our analyses.

2.2. *Quantitative paleoclimate estimates*

All floras analyzed in this study have previously published taxonomic assignments to the plant mega- or microfossils found at these sites (Supplementary Table S1). These taxonomic assignments allow us to use species probability density modeling of nearest living relatives (NLR) to constrain paleoclimate (Willard et al., 2019; West et al., 2020, 2021). In order to use NLRs of plant fossils to constrain paleoclimate, the assumption must be made that the range of environmental tolerance is determined by macroclimate (e.g., Reichgelt et al., 2018), or at least that biotic and abiotic tradeoffs within the plant group's niche space prevent the spread beyond certain macroclimatic thresholds. With probability density modeling of NLRs, an optimal macroclimatic range can be constrained for each plant group in an assemblage and by combining probabilities of macroclimatic range, an optimal range for the entire assemblage can be determined.

Here, optimal macroclimatic range of plant groups was determined by obtaining species geodetic occurrences from the Global Biodiversity Information Facility (GBIF.org, 2021; see Supplementary Table S2 for derived datasets of specific plant groups). The raw species occurrence data was filtered for exotic occurrences which may be unrepresentative of the natural climatic range of a plant group. Furthermore, plant occurrences tend to be recorded in larger density in more populous areas

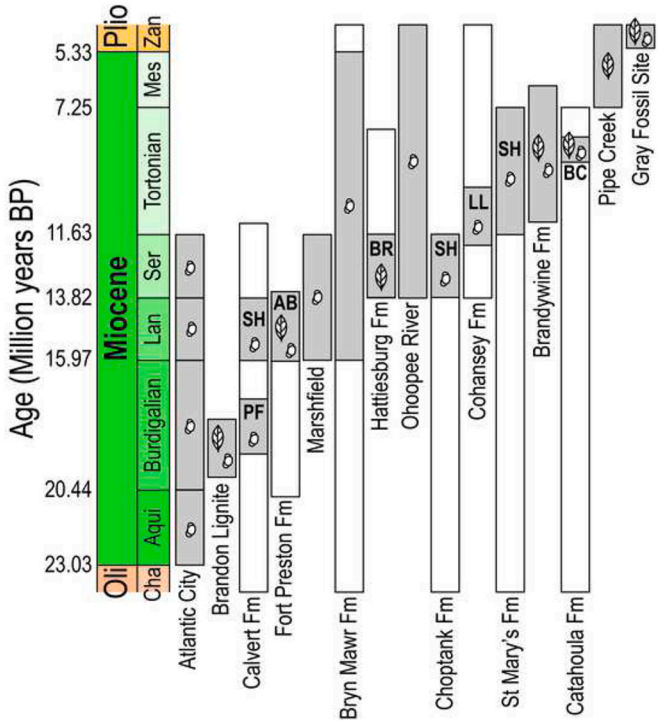

Fig. 2. Stratigraphic correlation of sedimentary formations in the eastern USA. Gray intervals indicate the best constrained time interval wherein a fossil flora was deposited, a pollen grain or leaf indicates whether the flora was composed of microfossils (pollen and spores), or megafossils (leaves, fruits and flowers) or both micro- and megafossils. Oli = Oligocene, Cha = Chattian, Aqui = Aquitanian, Lan = Langhian, Ser = Serravallian, Mes = Messinian, Plio = Pliocene, Zan = Zanclean, PF = Pollack Farm, SH = Stratford Hall, AB = Alum Bluff, BR = Bouie River, LL = Legler Lignite, BC = Big Creek / Chalk Hills.

and in more economically prosperous nations. To ascertain that our optimal climatic range calculations are not skewed as a result of spatially unequal sampling, we applied a random resampling approach. All but three random occurrences from every 0.1 × 0.1° and all but ten from every 1 × 1° grid cell were discarded. This approach retains some distribution skews that may arise from niche preference, while also preserving niche preference as a result of microclimates.

A consideration must be made whether all occurrences within a taxonomic group (e.g., a family or a genus) are given equal weighting in the optimal range calculation. The argument can be made that the species within a taxonomic group with the broadest distribution is the most successful, and therefore its disproportional representation within the larger plant group is appropriate. However, a species-weighted approach would give equal weight to each species, and is therefore more representative of the macroclimate space with the highest diversity. A distribution-weighted or species-weighted approach may yield a vastly different picture of the optimal macroclimatic range of a plant group, since the former would discount species with a restricted distribution.

In this study, we add a step to previous studies using probability density modeling of NLRs (Willard et al., 2019; West et al., 2020, 2021) to apply a species-weighted approach. This is achieved by extracting mean annual temperature (MAT), warmest (WQT) and coldest quarter mean temperature (CQT), mean annual precipitation (MAP) and driest month precipitation (DMP) for each geodetic datapoint for each species in a plant group. Climate data were extracted using the dismo package in R (Hijmans et al., 2017). All species with <5 occurrences, after the filtering process was applied, were considered too little data to calculate optimal climate range. The means and standard deviations of these extracted climatic values represent the optimal climate range of each species. For MAP and DMP, means and standard deviations are calculated from log-transformed values of actual MAP and DMP. A hundred resamples are then generated for each species for each climatic parameter. For example, if *Acer* (Sapindaceae) was identified in a fossil deposit, the means and standard deviation for MAT, WQT, CQT, MAP and DMP were calculated for each of its 88 species. Each species is then represented by 100 resamples, resulting, in this case, in 8800 total values for each climatic parameter. In this situation, even though *Acer platanoides* has 3046 and *Acer velutinum* has 5 occurrences, both are represented by 100 resamples. The means (μ_c) and standard deviations (σ_c) of each climatic variable are then calculated from the resamples for each taxa (t).

After the above described calculation for μ_c and σ_c, the process for calculating paleoclimate from NLRs is the same as in previous studies (Willard et al., 2019; West et al., 2020, 2021). A set of ~800,000 random unique combinations of MAT, WQT, CQT, MAP and DMP was generated. The likelihood (f) of a taxon occurring at any of these climate combinations by was determined calculating the product of probabilities for each climatic variable (c).

$$f(t_n) = \prod_{i=1}^{5} \pi \Big/ 2\sigma_c^2 \times e^{(x_c-\mu_c)/2\sigma_c^2} \quad (1)$$

Here, x_c is either MAT, WQT, CQT, MAP or DMP, and $f(t_n)$ is the joint likelihood of each taxon based on the five climatic variables. Then, the joint likelihood of occurrence of all taxa f(z) can be calculated for an assemblage (n), using the product of each $f(t_n)$.

$$f(z) = \prod_{i=1}^{n} f(t_n) \quad (2)$$

The combination of MAT, WQT, CQT, MAP and DMP with the highest probability density represents the most likely climate in which this fossil assemblage was growing. A 95% Confidence Interval is generated by calculating the maximum range of climatic variables with f (z) ≥ 5% of maximum f(z).

Two sets of climate reconstructions were made in this way: one from floral assemblages that include all taxa recovered at a site in a specific stage, and a second from floral assemblages that exclude taxa with a strong potential for an allochthonous source plant. This was achieved by eliminating taxa that were only identified from wind-dispersed pollen groups, including *Pinus*, *Abies*, *Picea*, *Alnus*, *Betula*, *Carya*, *Corylus*, *Fagus*, *Juglans*, *Zelkova*, *Ephedra*, *Liquidambar*, *Engelhardia*, *Platanus*, *Podocarpus*, *Pterocarya*, *Quercus*, *Salix*, *Sciadopitys*, *Taxodium*, *Tsuga*, *Myrica*, *Ostrya*, *Ulmus*, *Sequoia*, *Fraxinus*, *Populus*, *Cedrus*, Cyperaceae, Amaranthaceae and Poaceae. However, if those taxa were present at a site as macrofossils, such as vegetative material, infructescence or inflorescence, they were included in the analysis. In this second "locally-derived" analysis, sites that are described as deposited offshore were omitted entirely, including Stratford Hall, Atlantic City and Belvidere.

2.3. Proxy – Model paleoclimate intercomparison

Proxy reconstructions of Miocene climate in the eastern USA were compared to point extractions of an atmosphere-ocean coupled climate simulation (Supplementary Material). The paleolatitude and paleolongitude of each site were reconstructed for the middle of the site's potential depositional age using GPlates (Table 1), consistent with the paleogeographic boundary condition used in the simulation (Herold et al., 2008; Frigola et al., 2018). MAT and MAP were then extracted from the simulated Miocene terrestrial surface temperature and precipitation for sites that had an age overlap with the target time frame of the model simulation. The simulation targeted the Miocene Climatic Optimum (MCO, 14 to 18 Ma), which includes the depositional age of Alum Bluff, Brandon Lignite, Pollack Farm, Marshfield, the bottom section of Stratford Hall, and the top two sections of Atlantic City (Table 1). The simulation was carried out with the Community Earth System Model version 2 at 1.9 × 2.5° spatial resolution (Danabasoglu

et al., 2020) and featured similar model configurations as the Pliocene simulation using the same model (Feng et al., 2020). The end of run diagnostics of top of the atmosphere radiation imbalance and global mean surface temperature are provided in the supplemental material (Fig. S1). Root-Mean-Square Error (RMSE) was then calculated in order to compare model-proxy discrepancies.

$$RMSE = \sqrt{\sum_{i=1}^{n} \frac{\left(X_{model} - X_{proxy}\right)^2}{n}} \quad (3)$$

Proxy-model comparison was performed both on the analysis that includes taxa with a strong potential for long-distance dispersal and on the analysis that excludes these taxa (Section 2.2).

2.4. Vegetation clustering

In order to assess similarity between Miocene and modern vegetation types, 100 modern virtual vegetation plots were generated more or less equally distributed amongst the eastern forest regions (Dyer, 2006), including montane tropical forests in central America (Fig. 1). Modern vegetation sites were selected from preserves and parks. Eight were obtained from the CTFS-ForestGEO network (Anderson-Teixeira et al., 2015), seven montane forest sites from Veracruz with published species checklists of varying elevations (Williams-Linera et al., 2013), and the rest were obtained by determining a latitude/longitude centroid of the vegetation site and creating species checklists using a bounding box of 1 km^2 in the Global Biodiversity Information Facility (GBIF.org, 2021). From these checklists, invasive species were eliminated, and only plant groups that were also recorded at any of the fossil sites were included. A lower order taxonomic rank was used when higher order distinction was unavailable, for example in Rosaceae or Ericaceae. A total of 100 plant lists and corresponding vegetation types were assembled this way (Supplementary Table S3).

Simple absence/presence lists were then compiled of both the modern and fossil assemblages. Fuzzy cluster analysis (FCA) using the vegclust package (De Cáceres et al., 2010) in R (R Core Team, 2021) was then used to determine vegetation classification of modern and fossil assemblages. FCA has an advantage over other clustering methods in that it indicates the degree by which an object belongs to a cluster endpoint, rather than a binary result (De Cáceres et al., 2010). FCA using vegclust requires the user to predetermine the number of cluster endpoints. Here, we used the eastern forest types (Dyer, 2006) to set this predetermined number of clusters at eight, including northern hardwoods-conifer forest, oak-hickory forest, beech-maple-basswood forest, mesophytic-Appalachian forest, mesophytic-Acadian forest, southern mixed forest, subtropical evergreen forest and tropical montane forest. Tropical montane forest is not defined under the eastern forest types of Dyer (2006).

Two FCAs were performed with the abovementioned predetermined cluster endpoints. The first was “blind” in which pollen taxa with a high potential for long-distance dispersal were included and FCA was unsupervised, meaning that both modern and fossil plant assemblages could determine which group occupied the cluster endpoints. The second was “subjective” in which wind-dispersed pollen groups were excluded (Section 2.2) and FCA was supervised (Wiser and De Cáceres, 2013), meaning that only modern vegetation assemblages were used to determine cluster endpoints, and the best fit of fossil assemblages to those endpoints was then determined. A detrended correspondence analysis (DCA) was performed to determine the closeness of the fossil assemblages (without wind-dispersed elements) to modern-day vegetation groups.

3. Results

3.1. Proxy paleoclimate reconstructions

Reconstructed mean annual temperatures (MAT) for the Miocene eastern USA with long-distance pollen included in the analysis range from 12.3 °C for the Messinian – Zanclean Pipe Creek flora from Indiana to 20.2 °C for the Tortonian Big Creek flora from Louisiana (Supplementary Table S4). Warm quarter mean temperature (WQT) is consistently >20 °C, ranging from 20.7 °C at Pipe Creek to 25 °C at Big Creek (Supplementary Table S4). Cold quarter mean temperature (CQT) is more variable, as Big Creek and the Langhian Alum Bluff flora from Florida have reconstructed CQT of >14 °C, whereas Pipe Creek and the Tortonian Stratford Hall site from Virginia have CQT of <5 °C (Supplementary Table S4). The Serravallian Bouie River flora from Mississippi and Middle Miocene Marshfield site from Massachusetts are the only other sites with CQT of >10 °C. Mean annual precipitation (MAP) ranges between 98 cm yr^{-1} at Pipe Creek to 140 cm yr^{-1} at the Burdigalian Brandon Lignite flora from Vermont (Supplementary Table S4). Reconstructed driest month precipitation (DMP) suggests that there was some precipitation seasonality, with DMP at Big Creek ~20% of mean monthly precipitation (MMP) and DMP at the Serravallian-Tortonian Legler Lignite site from New Jersey ~50% of MMP (Supplementary Table S4). These climate ranges can be mostly classified as humid subtropical climates, although Alum Bluff, Big Creek and Bouie River may be classified as dry-winter humid subtropical climates, and Pipe Creek as a warm-summer humid continental climate (Supplementary Table S4, sensu Beck et al., 2018). The reconstructed biomes (Whittaker, 1962) are consistently in the range of Temperate Seasonal Forest (Fig. 3a), with the lower range of precipitation estimates in the Woodland biome.

Reconstructed MAT with long-distance pollen excluded is higher by an average of 1.7 °C (Table 2). All sites, except Alum Bluff, have higher reconstructed MATs using this method. Notably, reconstructed MAT of the Marshfield and the Burdigalian Pollack Farm site in Delaware increases by >3 °C with long-distance pollen excluded (Table 2). WQT with long-distance pollen excluded is higher by an average of 0.9 °C, and CQT is higher by an average of 2.4 °C (Table 2). CQT of the Brandon Lignite, Legler Lignite and Pollack Farm are also >10 °C, and Big Creek has a reconstructed CQT of >18 °C (Table 2). Changes to MAP are minor with an average increase of ~7 cm yr^{-1}, and DMP is similar as well, ranging from ~25% to ~60% of MMP. The same sites occupy the extremes (Table 2). With long-distance pollen excluded, climate classification (sensu Beck et al., 2018) mostly remains the same, although the upper temperature range now classifies Big Creek as a tropical savanna climate with dry winter characteristics (Table 2). This tropical savanna classification of Big Creek is also reflected in a shift towards the Tropical Savanna biome in the Whittaker (1962) classification (Fig. 3b). Hereafter, we will only focus on reconstructions derived from floras that were most likely autochthonously sourced (Table 2).

3.2. Comparison to modern

Discrepancies between modern and Miocene MAT are particularly evident north of 35°N in the Early to Middle Miocene (Fig. 4a). Notably, for the Miocene sites south of 35°N, MAT is similar or even lower than modern climates. Modern terrestrial MAT also has a distinct latitudinal gradient of ~0.9 °C per degree latitude along the US east coast, but the latitudinal gradient is flat for the Early to Middle Miocene MAT reconstructions (Fig. 4a), while Late Miocene MAT reconstructions follow a similar trend to modern (Fig. 4b). It has to be noted here that the absence of an Early to Middle Miocene latitudinal gradient in this dataset could be the result of Miocene floras having formed at different times within this timespan (Table 1), featuring different global climate regimes (e.g., Westerhold et al., 2020; see also Section 3.3). Similar to MAT, reconstructed CQT contrasts notably with modern CQT north of 35°N (Fig. 4c). However, Miocene sites south of 35°N are not cooler than

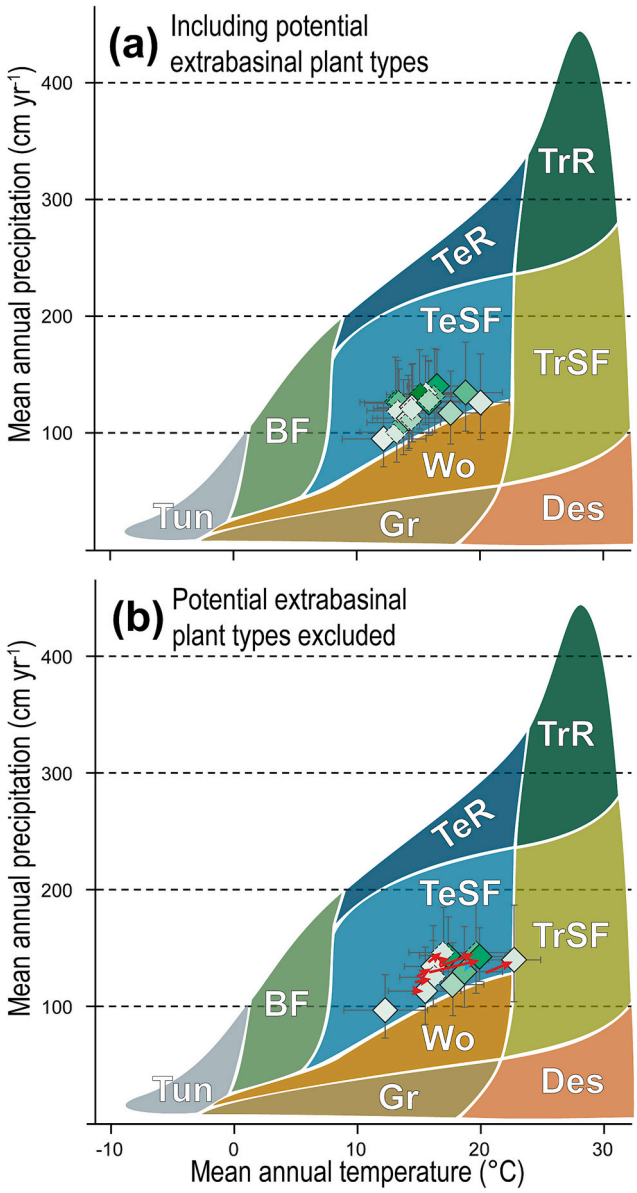

Fig. 3. Whittaker (1962) biome plots. (a) All Miocene eastern USA sites studied here (Supplementary Table S4) including microfossil only (small dashed diamonds) and sites that include megafossils (large diamonds). (b) Miocene eastern USA sites with plant types with a high potential for extrabasinal sourcing only identified from microfossils excluded (Table 2). Red arrows indicate that the reconstructed temperature is warmer than the reconstruction with all plant types included (a). The color gradient of the diamonds corresponds to the age of the flora, from Early (dark green) to Late Miocene (light green). All Tun = Tundra, Gr = temperate grassland or cold desert, BF = boreal forest, Wo = Woodland or shrubland, Des = Subtropical desert, TeSF = Temperate seasonal forest, TeR = Temperate rainforest, TrSF = Tropical seasonal forest or savanna, TrR = Tropical rainforest. (For interpretation of the references to colour in this figure legend, the reader is referred to the web version of this article.)

modern climates, but more similar or even warmer in the case of Big Creek. The Early to Middle Miocene CQT latitudinal gradient is also flat (Fig. 4c), while again for the Late Miocene the latitudinal gradient is similar to modern, albeit with somewhat higher CQT (Fig. 4d).

At sites north of 35°N, reconstructed Miocene MAP is higher than modern, with the exception of the Pipe Creek and Bradywine sites (Fig. 4e,f). Miocene sites south of 35°N all have a very similar reconstructed MAP to modern. Modern MAP decreases towards high latitudes at a rate of ~2.7 cm yr^{-1} per degree latitude (Fig. 4e,f). However, this latitudinal gradient is not evident in the Miocene (Fig. 4e,f). Reconstructed DMP as a proportion of MMP is consistently lower from modern (Fig. 4g,h) indicating enhanced precipitation seasonality in the Miocene compared to today. All sites, except the Legler Lignite and Pollack Farm sites, have DMP/MMP more similar to modern-day Florida climates. Modern day DMP/MMP increases with latitude at a rate of ~2% per degree latitude, but this trend is not evident in the Miocene data (Fig. 4g, h).

3.3. Proxy-model comparison

Comparing proxy-derived MCO estimates to a MCO climate model reveals a large proxy-model MAT discrepancy in the eastern USA (RMSE = 10.1 °C; Fig. 5a). This discrepancy is improved with the exclusion of long-distance pollen (RMSE = 6.7 °C, Fig. 5b). However, terrestrial MAT proxy reconstructions are still consistently lower than modeled reconstructions, regardless of the exclusion of long-distance pollen. This discrepancy likely suggests overestimates of mid-Miocene warming by this model configuration. There is more agreement between proxy and model MAP reconstructions (RMSE = 23 cm yr^{-1}; Fig. 5c). Proxy-model agreement improves with the exclusion of long-distance pollen (RMSE = 4 cm yr^{-1}; Fig. 5d). This MCO proxy-model comparison has a limited amount of datapoints, but is useful in highlighting the disagreement in reconstructed MAT, agreement in reconstructed MAP, and improved agreement when extrabasinal plant fossils are excluded from the analysis.

3.4. Vegetation type

Vegetation clustering using FCA generally grouped modern virtual vegetation plots together by the correct biogeographic region (Supplementary Table S5 & S6). Subtropical evergreen plots all fell in the same cluster, albeit mixed with several Southern Mixed plots (Fig. 6a,b). Tropical montane plots were mostly consistent, clustering closest to the Subtropical evergreen cluster, and with a Southern mixed site clustering with the Tropical montane sites (Fig. 6a,b). The Northern hardwoods-conifers plots were consistently clustered as well, and in the unsupervised cluster with palynofloras included, clustered close to a group of fossil sites (Fig. 6a). This likely is the result of the prevalence of Northern hardwoods and conifers in the palynofloras and why NLR paleoclimate reconstructions from palynofloras generally provide lower temperature reconstructions (Fig. 3a,b). FCA could not recognize the Mississippi alluvial vegetation type (Dyer, 2006), instead placing these plots with Southern mixed or Oak-hickory forests (Fig. 6a,b). Oak-hickory and Mesophytic-Appalachian were mostly mixed together, whereas Beech-maple-basswood and Mesophytic-Acadian in both supervised and unsupervised FCA formed a distinct cluster (Fig. 6a,b). DCA (Supplementary Table S7) broadly matches the results of FCA, with distinct clusters for Tropical montane, Subtropical evergreen and Northern hardwoods-conifers plots (Fig. 6c). Southern mixed, Mesophytic and Beech-maple-basswood plots have some overlap with other clusters, but are fairly distinct, while Oak-hickory and Mississippi alluvial do not form distinct clusters (Fig. 6c).

As noted above, the unsupervised FCA with wind-dispersed pollen included (Supplementary Table S5), groups all palynofloras together, making interpretation of their vegetation types problematic (Fig. 6a). With wind-dispersed pollen excluded (Supplementary Table S6), the Legler Lignite site clusters with Mesophytic-Acadian forests, whereas Marshfield and Pollack Farm group between the Subtropical evergreen and Tropical montane clusters (Fig. 6b). However, the DCA reveals that the Legler Lignite, Marshfield and Pollack Farm sites are not close to any modern vegetation types (Fig. 6c), and the supervised clustering may show the most similar modern eastern North American forest types, while still not being very similar. Additionally, these three sites are palynofloras with wind-dispersed pollen excluded, which may still not

Table 2
Results of nearest living analysis of plant fossils recovered from Miocene fossil localities of the eastern USA, with extrabasinal plant groups excluded. For results with extrabasinal plant groups included, see Supplementary Table S4. N = number of different taxa used in nearest living relative analysis (see Table S1). MAT = mean annual temperature, WQT = warmest quarter mean temperature, CQT = coldest quarter mean temperatures, MAP = mean annual precipitation, DMP = driest month precipitation. Broad biome classification follows Whittaker (1962) and climate classification follows Beck et al. (2018). Cfa = temperate climate + no dry season + hot summer, Cwa = temperate climate + dry winter + hot summer, Aw = tropical climate + savannah, Dfb = cold climate + no dry season + warm summer. Note that sites with the potential classification of Cwa are only classified as such if summer is the wet season.

Site name	N	MAT (°C)	WQT (°C)	CQT (°C)	MAP (cm)	DMP (cm)	Class (Whittaker)	Class (Köppen-Geiger)
Brandon Lignite (VT)	22	17.4 ± 2.4	23.5 ± 2.2	11 ± 3.6	143 + 33/−27	4 + 3/−1	Seasonal Forest	Cfa
Legler Lignite (NJ)	10	17 ± 2.8	23.2 ± 2.7	10.5 ± 4.5	146 + 38/−31	7 + 3/−2	Seasonal Forest	Cfa
Alum Bluff (FL)	25	18.6 ± 3.2	24.2 ± 2.2	13 ± 4.8	129 + 39/−30	3 + 3/−1	Seasonal Forest / Woodland	Cfa/Cwa
Pollack Farm (DE)	11	19.9 ± 2.1	25.7 ± 1.2	14.5 ± 3	142 + 26/−21	7 + 2/−2	Seasonal Forest	Cfa
Big Creek & Chalk Hills (LA)	16	22.7 ± 2.1	26.1 ± 1.6	18.9 ± 3.1	139 + 48/−35	3 + 3/−2	Seasonal Forest / Woodland / Tropical Savanna	Cfa/Cwa/ Aw
Ohoopee River (GA)	16	16.2 ± 2.7	22.5 ± 2.3	9.8 ± 3.9	125 + 31/−25	4 + 3/−2	Seasonal Forest	Cfa
Brandywine (MD)	29	15.4 ± 3	22.5 ± 2.4	7.5 ± 4.4	112 + 39/−28	3 + 2/−2	Seasonal Forest	Cfa
Gray Fossil Site (TN)	26	16.4 ± 2.4	23.6 ± 2.0	8.8 ± 3.5	136 + 38/−29	4 + 3/−1	Seasonal Forest	Cfa
Pipe Creek (IN)*	26	12.6 ± 3.4	20.6 ± 2.6	4.8 ± 4.9	96 + 33/−25	3 + 3/−1	Seasonal Forest / Woodland	Cfa/Dfb
Bouie River (MS)*	18	17.8 ± 2.5	24.4 ± 2.1	10.3 ± 3.7	118 + 35/−27	2 + 3/−1	Seasonal Forest / Woodland	Cfa/Cwa
Marshfield (MA)	11	19.6 ± 2.8	24.2 ± 2.4	15 ± 4.2	146 + 45/−35	5 + 4/−2	Seasonal Forest	Cfa

* Only megafossils: results in this table and Table S4 are the same.

provide a local floral signal as a megaflora would.

Fossil sites with megafloral remains more consistently clustered with specific vegetation types (Supplementary Table S5), suggesting that they are compositionally similar to modern vegetation types. In FCA, the Alum Bluff and Brandywine sites clustered with the Southern Mixed vegetation forest type (Fig. 6b), which was consistent with DCA (Fig. 6c). It should be noted that Alum Bluff and Brandywine did not cluster closely to the Subtropical Evergreen forests, but rather appeared to be more similar to the Mississippi alluvial vegetation type. The Alum Bluff and Brandywine sites are spatially and temporally disparate, deriving from the Langhian of Florida and the Late Miocene of Maryland, respectively (Table 1). Southern Mixed forest occurs in northern Florida and southern Maryland today as well (Dyer, 2006), and therefore the data presented here do not present a notable range change of this vegetation type.

The Bouie River and Pipe Creek sites clustered with the Beech-maple-basswood forest type, both in the FCA (Fig. 6b) and the DCA (Fig. 6c). Again, Bouie River and Pipe Creek are spatially and temporally disparate, deriving from the Serravallian of Mississippi and the Messinian or Early Pliocene of Indiana (Table 1). Natural vegetation in Indiana today is largely Beech-maple-basswood forest; however, the occurrence of Beech-maple-basswood forest in the Serravallian of Mississippi would represent a further southward distribution than modern of this vegetation type (Dyer, 2006).

The Big Creek, Brandon Lignite and Gray Fossil sites cluster with the Subtropical evergreen and Tropical montane forests with FCA (Fig. 6b). With DCA, these sites are similar to Subtropical evergreen forests too, especially the Gray Fossil site which also overlaps with the Southern mixed forest cluster (Fig. 6c). The Ohoopee River site floral composition is only based on pollen types, as are the Legler Lignite, Marshfield and Pollack Farm sites. Therefore, despite Ohoopee River clustering with Subtropical evergreen and Tropical montane forests in FCA (Fig. 6b), the vegetation type at this location is spurious. Vegetation with affinities to modern-day Subtropical evergreen or Tropical montane forests at the Brandon Lignite and Gray Fossil sites represents northward expansion of these vegetation types in the Miocene. Subtropical evergreen forests are currently only found in Florida and southeast USA coastal forests, whereas Tropical Montane forests occur at intermediate altitudes (1–2.5 km above mean sea level) in Mexico (Fig. 1). Subtropical evergreen or tropical montane forests at the Brandon Lignite site indicates a northward expansion of at least 12° during the Burdigalian relative to today and presence at the Gray Fossil site a northward expansion of at least 2° during the Zanclean.

4. Discussion

4.1. Poleward amplification

Our terrestrial quantitative paleoclimate estimates on Miocene fossil plant remains from the eastern USA allowed us to gain a spatial as well as a temporal perspective. According to these reconstructions, Miocene terrestrial climate of the eastern USA was similar to modern south of 35°N, but was both wetter and warmer than modern north of 35°N (Fig. 4). This suggests poleward amplification of temperature affects the North American east coast during the greenhouse climate states of the Miocene. Poleward amplification of temperatures agrees with modeled climate reconstructions of the Miocene (You et al., 2009; Herold et al., 2010; Goldner et al., 2014; Burls et al., 2021) as well as modern-day climate observations and modeled future climate scenarios (e.g., Bekryaev et al., 2010; Smith et al., 2019). A weaker than modern Middle and Late Miocene meridional temperature gradient was also found for amalgamated continental climate reconstructions spanning North America and western Eurasia (Utescher et al., 2017). The absence of an Early to Middle Miocene meridional temperature gradient in our reconstructions (Fig. 4a) may suggest potentially intensified latitudinal heat transport by the Gulf Stream at this time, given the much warmer reconstructed SSTs (28 °C) in the North Atlantic (Super et al., 2018; Guitián et al., 2019). Additionally, higher than modern MAP north of 35°N (Fig. 4e) may indicate enhanced moisture transport during the Early to Middle Miocene that accompanied poleward amplification. Increased rainfall in northeastern states, but not in southeastern states, has also been observed in precipitation data of the last century (Peterson

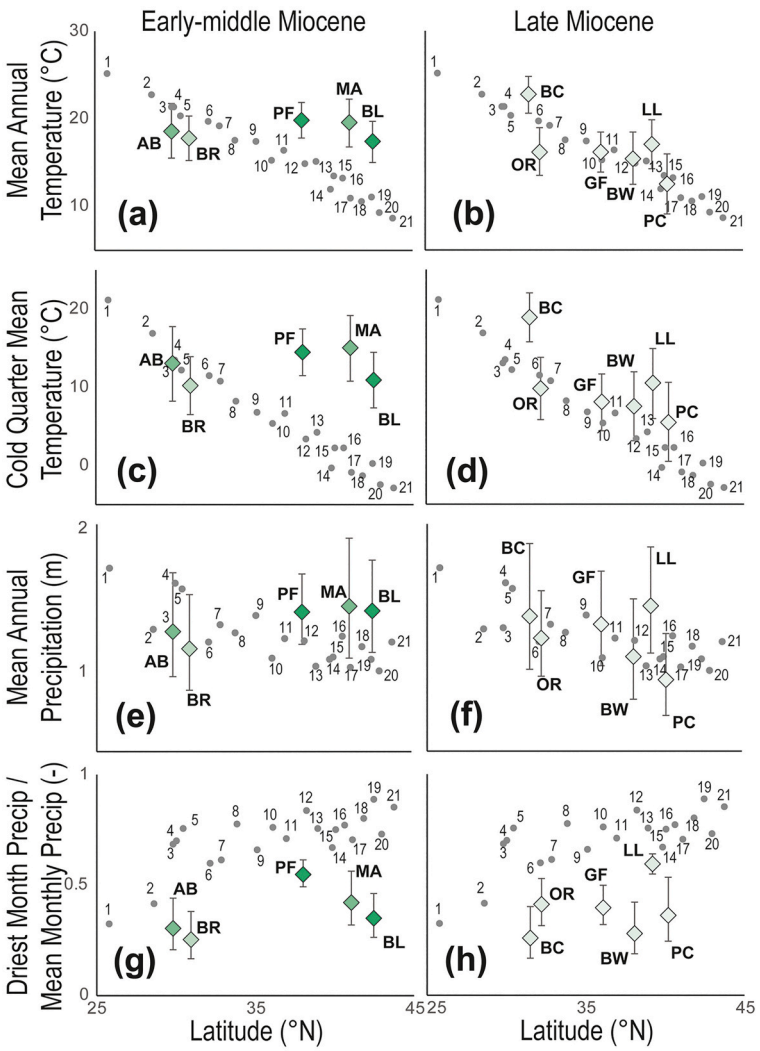

Fig. 4. Climate comparison of Early to Middle Miocene (a,c,e,g) and Late Miocene (b,d,f,h) sites to modern: (a,b) mean annual temperature, (c,d) cold quarter mean temperature, (e,f) mean annual precipitation, (g,h) driest month precipitation / mean monthly precipitation. Modern comparison (gray circles): 1 = Miami FL, 2 = Orlando FL, 3 = Houston TX, 4 = New Orleans LA, 5 = Baton Rouge LA, 6 = Savannah GA, 7 = Charleston SC, 8 = Atlanta GA, 9 = Memphis TN, 10 = Greensboro NC, 11 = Norfolk VA, 12 = Louisville KY, 13 = Washington DC, 14 = Indianapolis IN, 15 = Philadelphia PA, 16 = New York City NY, 17 = Akron OH, 18 = Hartford CT, 19 = Boston MA, 20 = Buffalo NY, 21 = Portland ME. Fossil sites (diamonds) are graded from darker to lighter green indicating earlier to later in the Miocene, same as the timeline in Fig. 2: AB = Alum Bluff FL, BR = Bouie River MS, BC = Big Creek/Chalk Hills LA, OR = Ohoopee River GA, GF = Gray Fossil site TN, BW = Brandywine MD, PF = Pollack Farm DE, LL = Legler Lignite NJ, PC = Pipe Creek IN, MA = Marshfield MA, BL = Brandon Lignite VT. (For interpretation of the references to colour in this figure legend, the reader is referred to the web version of this article.)

et al., 2013; Easterling et al., 2017) and is predicted to continue during the 21st century (Easterling et al., 2017). Terrestrial Miocene climate reconstructions from the eastern USA based on paleobotanical proxies therefore provide empirical support that poleward amplification of temperature and precipitation occurs during warmer than modern global climates.

Taken together, the Miocene climate in comparison to modern of the eastern USA can be described as a northward expansion of the warm-temperate, fully humid, hot summer climate type that prevails in the southeast USA today (Köppen-Geiger classification Cfa, Rubel et al., 2017), replacing the snow, fully humid, warm or hot summer climate type of the northeast USA (Köppen-Geiger classification Dfa or Dfb, Rubel et al., 2017). Indeed, this climate transition is also predicted to develop over the next century (Rubel and Kottek, 2010).

4.2. Seasonality

In the warmer conditions of the Miocene, seasonal temperature differences in the eastern USA were smaller than modern (Table 2), whereas seasonal precipitation differences were larger (Fig. 4g,h). Little contrast between the Miocene and modern is observed south of 35°N for MAP and MAT; however, Miocene DMP/MMP reconstructions are lower for every site (Fig. 4g,h) implying precipitation seasonality similar to modern-day southern Florida. From this data, it is not clear which month was the driest, but modern-day Florida has drier winters than summers. Fall precipitation in the eastern USA has undergone the most consistent and uniform increase over the last century (Peterson et al., 2013). Future projected changes are expected to see significant precipitation increases in winter and spring, in particular throughout the northeast and likely in the form of snow (O'Gorman, 2014), although as the climate continues to warm, winter and spring temperatures are expected to be too warm for snow (Ning and Bradley, 2015; Easterling et al., 2017).

Wetter summers and drier winters have been inferred from lacustrine rhythmites at the Gray Fossil Site in Tennessee (Shunk et al., 2009a). Conversely, the Pipe Creek Sinkhole was interpreted to be deposited in a Mediterranean-style climate, with hot and dry summers and cool and wet winters, based on paleosol type (Shunk et al., 2009b). Importantly, the Pipe Creek Sinkhole study by Shunk et al. (2009b) covers several stratigraphic intervals, with variable facies, and the facies that the flora was recovered from indicates a wetter local paleoenvironment than the terra rosa paleosol that the Mediterranean climate interpretation was based on. The interpretation of Shunk et al. (2009b) of a more continental climate at Pipe Creek is supported by our data, which has the lowest MAP reconstruction (Table 2) and in the Whittaker (1962) biome plot is reconstructed as straddling the temperate seasonal forest and woodland biomes (Fig. 3). However, the Pipe Creek flora was deposited in the Late Miocene, which was a time of global cooling and expansion of drier continental climates (Herbert et al., 2016), and it is therefore unclear whether a coast-to-inland precipitation gradient would have existed during the warmer Early and Middle Miocene.

In the western continental USA, $\delta^{18}O$ measurements from paleosols and clays show drier winter conditions leading to an open habitat

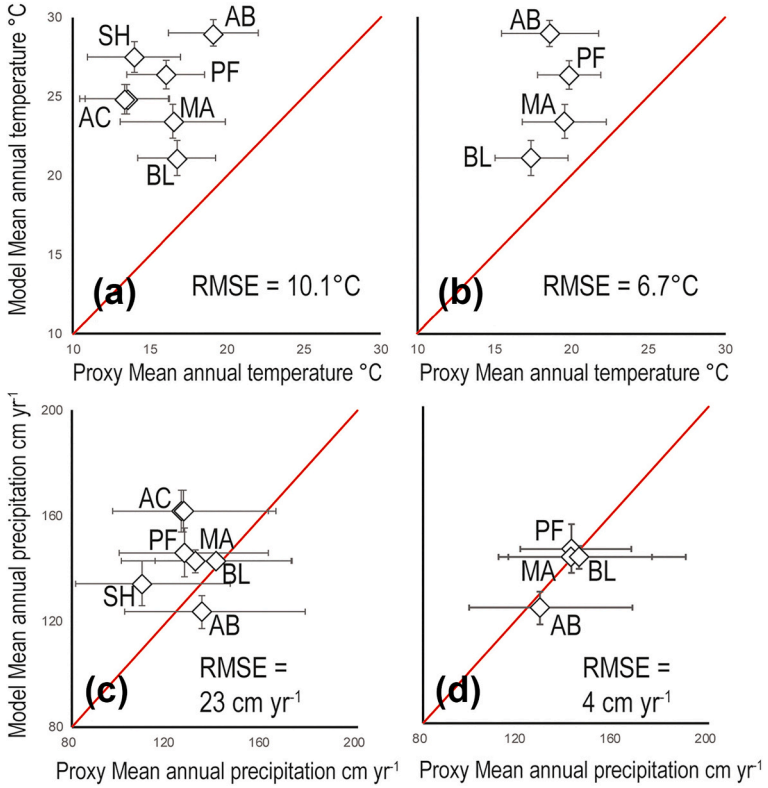

Fig. 5. Model – proxy comparison of sites deposited during the Middle Miocene Climatic Optimum in this study. RMSE = root mean squared error. (a, c) includes plant types in the proxy reconstructions that are potentially extrabasinally derived, (b, d) excludes extrabasinal input.

expansion in the Late Oligocene into the Miocene (Kukla et al., 2022). The study of Kukla et al. (2022) also shows that the summer to winter precipitation contrast was more pronounced east of the Rocky Mountains continental divide, with a potentially delayed transition to drier winters relative to farther west. A Miocene transition to more seasonal precipitation regimes is not obvious from our data (Table 2, Fig. 4g,h). A north-south gradient may exist with a higher DMP/MMP at northern sites than at southern sites (Fig. 4g,h), although the datapoints are too sparse and ages poorly resolved in order to establish a trend. Potentially, an eastern USA seasonality transition occurs earlier, in the Aquitanian or in the Late Oligocene. However, offshore vegetation and climate reconstructions of the Oligocene – Miocene also do not show a drastic change in vegetation (Kotthoff et al., 2014).

A potential mechanism for higher-than modern Miocene summer rainfall in the eastern USA is enhanced extreme precipitation events. Atmospheric moisture carrying capacity is correlated with temperature and in summer the air can get saturated through evaporation and transpiration. Elevated temperatures therefore increase the chance of extreme precipitation events, as has been the case for summer and especially fall in the eastern USA over the last century (Easterling et al., 2017). Additionally, the eastern USA is prone to extreme precipitation events due to landfall of tropical cyclones. In general, tropical cyclones are expected to increase in intensity, and the season in which tropical cyclones may occur in the USA is expected to lengthen in a warmer world (Knutson et al., 2015; Walsh et al., 2015; Levin and Murakami, 2019). In addition, climate models of the hothouse world in the Eocene suggest greater tropical storm intensity and reach in North America (Kiehl et al., 2021). Enhanced moisture transport due to changes in or intensifying storm tracts have been suggested for Miocene greenhouse climates as well (Böhme et al., 2008; Micheels et al., 2011).

4.3. Proxy – Model mismatches

Early studies identified mismatches between zonal means of paleofloral proxies and model simulations in western Eurasia and western North America (Utescher et al., 2017). In the eastern USA, there is also a strong mismatch between MAT reconstructions from the plant-based proxy used in this study and MAT produced by CESM2 at 2° spatial resolution (Fig. 5a,b). This mismatch is reduced by removing plants and localities from the analysis with a strong potential for the inclusion of extrabasinal elements (Fig. 5b), but the model still produces a MAT that is on average > 6 °C warmer than the terrestrial MAT reconstructions. The mismatch between terrestrial proxy reconstructions and modeled temperatures has been problematic for model-proxy intercomparison projects (e.g., Utescher et al., 2017; Burls et al., 2021).

Proxy-based Miocene SST reconstructions from the North Atlantic are mismatched with our terrestrial MAT reconstructions as well. Reconstructions from DSDP site 608 (42.837, −23.088) suggest SSTs from the interval of deposition coeval with that of the Brandon Lignite of 30.0 ± 2.9 °C (TEX_{86}) and 26.5 ± 2.0 °C (U^{K}_{37}) (Super et al., 2018). IODP site U1406A, which is closer to the US east coast (40.35, −51.65), has reconstructed SSTs for the same time interval of 25.4 ± 1.7 °C (TEX_{86}) and 27.7 ± 2.0 °C (U^{K}_{37}) (Guitián et al., 2019). This would mean that terrestrial MAT at the Brandon Lignite site is 8–12 °C colder than SSTs in the North Atlantic at similar latitudes. The same SST records are also warmer than Marshfield (5.8–7.8 °C), Legler Lignite (7.9–10.5 °C) and Pollack Farm (5.5–12.0 °C), for the respective time intervals that these sites were deposited. No SST reconstructions existed for the North Atlantic at similar time intervals and/or similar latitudes for the other eastern USA sites studied here. On the surface, these differences between terrestrial MAT and SST may suggest problems in reconstructions. However, modern average annual SST can be higher than US east coast MAT as well. For example, SST from the Gulf Stream (Hurrell et al., 2008) is consistently warmer than terrestrial east coast MAT (Hijmans

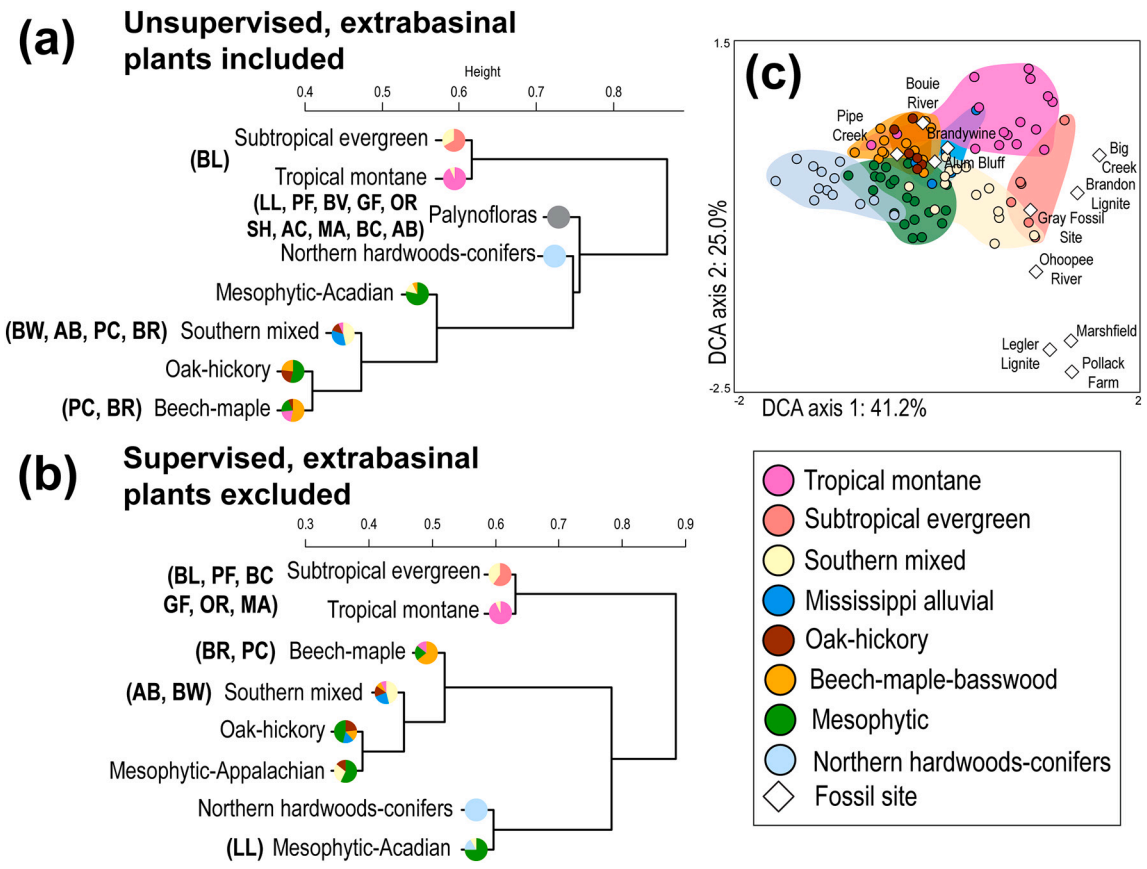

Fig. 6. Result of fuzzy cluster analysis (FCA, a,b) and detrended correspondence analysis (DCA, c), showing matching of fossil floras with modern forest types based on composition. Pie-charts at cluster tips indicate the percentage of modern vegetation assemblages (sensu Dyer, 2006) that contribute to that cluster endpoint. BL = Brandon Lignite, LL = Legler Lignite, PF = Pollack Farm, BV = Belvidere, GF = Gray Fossil site, OR = Ohoopee River, SH = Stratford Hall, AC = Atlantic City, MA = Marshfield, BC = Big Creek/Chalk Hills, AB = Alum Bluff, BW = Brandywine, PC = Pipe Creek, BR = Bouie River.

et al., 2017) at the same latitude; by up to 10 °C at 44°N. The Miocene east coast terrestrial MAT – SST discrepancy is therefore reconcilable with modern-day processes, such as ocean heat transport. Though as Super et al. (2018) points out, Middle Miocene SST at DSDP site 608 was nearly 15 °C warmer than today, indicating enhanced northward heat transport. Consistent with this result, our terrestrial MAT also shows amplified warming in the high latitudes. Taken together, the differences between reconstructed terrestrial MAT and SST may suggest a similar land-sea thermal contrast to today along the North American east coast.

Curiously, Miocene terrestrial MAT may be consistently lower than coeval SST reconstructions in Northern Hemisphere mid-latitudes (Fig. 7a,b), but SST overlaps with reconstructed terrestrial WQT (Fig. 7c,d). This could be attributable to a combination of the greater seasonality and colder winter on land compared to the ocean in general and the aforementioned northward heat transport by ocean currents.

Terrestrial NLR-based MAT reconstructions from the eastern USA presented in this study are consistent with MAT reconstructions using the Climate Leaf Analysis Multivariate Program (CLAMP) from western North America and Europe (Fig. 7a,b). Additionally, with the exception of reconstructions of high-altitude floras in the Miocene Rocky Mountains (Wolfe et al., 1997), North American and European plant-based terrestrial MAT reconstructions appear to follow a latitudinal trend, both for the warmer Early-Middle Miocene (Fig. 7a) and the Late Miocene (Fig. 7b). Though also relying on plants, CLAMP is independent of taxonomy, relying instead on what are accepted universal physiological responses expressed in the phenotypes of angiosperm leaves to macroclimate variation (Yang et al., 2015; Spicer et al., 2020). As such, CLAMP reconstructions are independent of those based on NLR, and the similarity of zonal MAT reconstruction of these two proxies (Fig. 7a,b) suggests that the records presented in this study are not anomalous. In addition, NLR- and CLAMP-based paleoclimate reconstructions from single localities show agreement in reconstructed MAT (e.g., Reichgelt et al., 2015; West et al., 2020; Reichgelt et al., 2022), though in some European studies, mismatches between NLR- and CLAMP-based paleoclimate reconstructions were identified (e.g., Uhl and Herrmann, 2010; Kvaček et al., 2014; Moraweck et al., 2015). More rarely and more variably, terrestrial MAT reconstructions based on soil carbonate clumped isotopes and NLR are usually harmonious (Hyland et al., 2018; Methner et al., 2020). The terrestrial temperature reconstructions based on soil carbonate clumped isotopes of the Miocene that are laterally closest to our paleobotanical reconstructions are in Texas (at 28°N). The Texas clumped isotope reconstructions give soil temperatures, representative of MAT or mean warm season air temperature, of 24–28 °C (Fig. 7b, Godfrey et al., 2018), which overlaps with our reconstruction at Big Creek (MAT = 22.7 ± 2.1 °C).

4.4. Plant nearest living relatives in paleoclimate reconstructions

Plant fossil-based terrestrial paleoclimate reconstructions are increasingly used in global proxy-model intercomparison projects (e.g., Carmichael et al., 2016; Burls et al., 2021; Hutchinson et al., 2021). NLR techniques, specifically the Coexistence Approach, have been strongly criticized for subjectivity, poor use of statistics, and opaque NLR data (Grimm and Potts, 2016; Grimm et al., 2016). Novel NLR techniques, such as the one used in this study, have attempted to tackle these issues through, for example, the usage of probability density modeling and using public and continuously updated NLR data sources (e.g., the Global Biodiversity Information Facility, GBIF.org, 2021). Nevertheless,

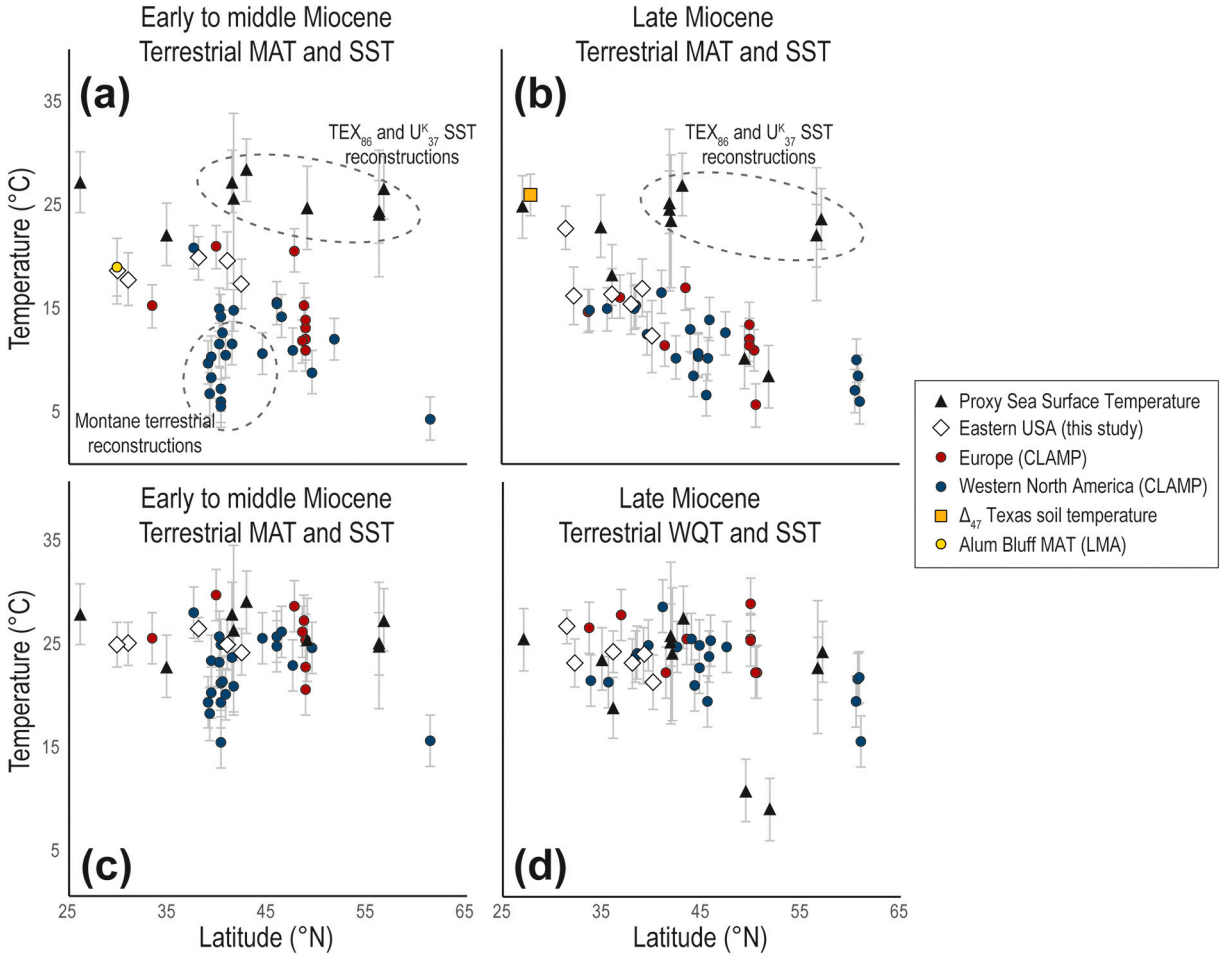

Fig. 7. Comparison between previously published sea surface temperatures (SST), mean annual temperature (MAT, a,b) and warmest quarter mean temperature (WQT, c,d), for the Early to Middle Miocene (a,c) and Late Miocene (b,d). Sources of temperatures in this figure can be found in Supplementary Table S8. CLAMP = climate leaf analysis multivariate program, LMA = leaf margin analysis, Δ47 = carbonate clumped isotopes.

as NLR techniques are some of the most common sources of terrestrial paleoclimate estimates that are increasingly compared with other proxy and model results, it is useful to review and discuss potential sources of systematic bias. The four sections below outline four observed or theoretical sources of bias in NLR-based MAT reconstructions. We provide a brief discussion of how such biases have been addressed or might be addressed in the future.

4.4.1. *Extrabasinal plant inclusion*

NLR-based paleoclimate reconstructions often rely on taxonomic identifications based on pollen and spores (e.g., Ivanov et al., 2011; Pross et al., 2012; Willard et al., 2019; Huurdeman et al., 2021; Thompson et al., 2022). Using pollen and spores for quantitative paleoclimate reconstructions is advantageous, because pollen and spores are far more abundant than other plant fossils, readily identifiable to a plant group, and are dispersed to marine sediments. Moreover, where megafossil assemblages usually offer no more than a 'snapshot' of climate in time, pollen and spore assemblages can be used to reconstruct transient climate states (e.g., Kotthoff et al., 2014; Prader et al., 2017, 2020). However, pollen and spore relative abundance is strongly dependent on dispersal syndrome and, where studied, significant mismatches occur between megafloras and palynofloras (e.g., Mildenhall et al., 2014; Lowe et al., 2018; Lott et al., 2019). Megafloras tend to be locally derived, with large organs, such as fruits and leaves, that do not transport over long distances before disintegrating. However, pollen and spores, especially those adapted for wind pollination, can become part of a microfloral assemblage while not representing the local paleoenvironment (McGlone et al., 1996; Jackson and Williams, 2004; Mander and Punyasena, 2018). This inclusion of extrabasinally-derived pollen and spores generates an apparent climate envelope in NLR analysis that is colder than the true climate of the depositional environment (Fig. 8a), since the wind-dispersal pollination syndrome tends to be more abundant in cooler climates (Regal, 1982; Rech et al., 2016).

In this study, when plant types were omitted that were potentially extrabasinally-derived, the reconstructed temperature as well as the reconstructed precipitation increased (Fig. 3). Though in the case of the southernmost site, Alum Bluff, this change made little difference (Table 2 and Supporting Information Table S4). Some NLR-based paleoclimate studies using microfossils choose to omit plant groups that tend to dominate the pollen assemblage but are unrepresentative of local vegetation (e.g., Willard et al., 2019). In other studies, a 'critical abundance' threshold is applied, wherein the presence of a particularly abundant plant group in NLR analysis is only considered if it is above a certain relative abundance that would imply local presence (Huurdeman et al., 2021; Allstädt et al., 2021).

4.4.2. *Selective extinction*

Paleofloras include plants with both known and unknown taxonomic affinities (e.g., Lott et al., 2019). The older the paleoflora, the more likely it is that there are no known modern analogues for species that occur in, or even dominate the assemblages, possibly because the lineage is extinct. By definition, the species that are present today represent lineages that survived, and therefore were able to adapt and thrive in modern-day climate conditions. The plants in a fossil assemblage could

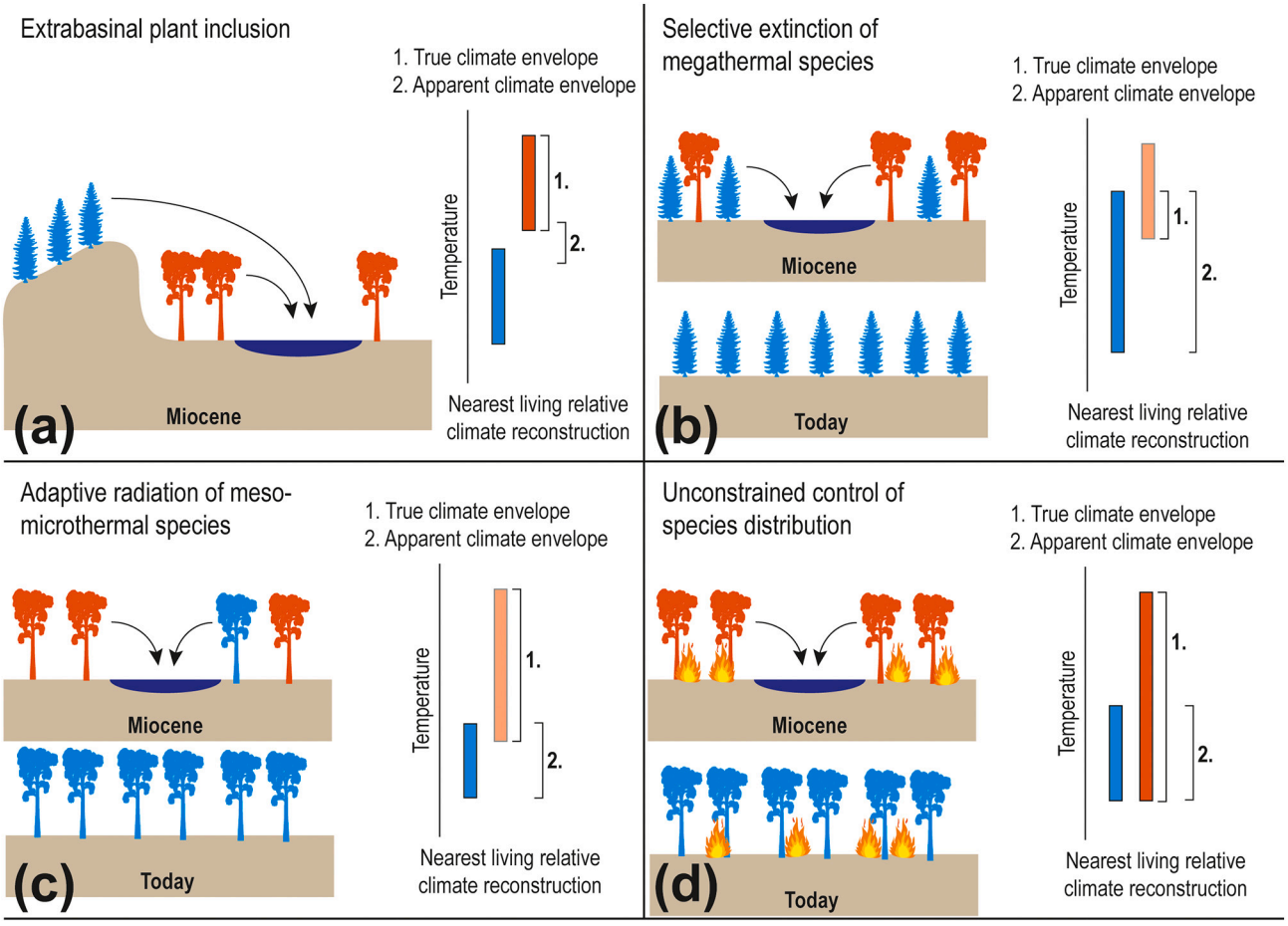

Fig. 8. Schematic representation of the hypothetical sources of reconstruction bias in nearest living relative-based (NLR) approaches based on fossil plants, including the effect it could have on a temperature reconstruction. (a) The inclusion of extrabasinal plants, commonly through wind-dispersed pollen, will generate a cooler apparent climatic envelope. (b) Selective extinction of plant groups with a preference for warmer climates may result in a cooler climatic envelope. (c) Adaptive radiation of species with a tolerance for cooler climate may result in a cooler climatic envelope. (d) Macroclimate is not the determining factor of vegetation distribution, but rather an environmental factor such as fire or edaphic conditions controls vegetation, resulting in no apparent difference between the Miocene and modern climatic envelope.

therefore be made up partially of plant groups that had a broad climatic tolerance and survived to this day, and plant groups with a narrower climatic tolerance that went extinct. For example, the global cooling trend since the Middle Miocene (e.g., Westerhold et al., 2020) may have led to selective extinction of megathermal species, leaving only cold-tolerant species to define the climate envelope (Fig. 8b).

The problem of selective extinction is of particular concern in paleoclimates potentially lacking a modern analogue. For example, tropical latitudes during greenhouse and hothouse climates are notoriously problematic for proxies that rely on modern-day climates for calibration. Do relatively cool terrestrial climates at the tropics during global hothouse conditions indicate a drastic change in global atmospheric circulation systems and non-linear temperature responses, or vegetation assemblages and leaf physiognomy without a modern analogue (e.g., Yao et al., 2009; Spicer et al., 2014; Shukla et al., 2014; Xie et al., 2019)? Similar problems are prevalent in temperature proxies that rely on organic geochemistry (e.g., Peterse et al., 2012), and the most commonly advocated solution is to apply a multi-proxy approach, whenever possible (Hollis et al., 2019).

In terrestrial paleoclimate studies that focus on high-to-mid-latitude locations during global green- or hothouses, the problem of non-analogue temperature states is not as prevalent. This is because there is no restriction to northward migration of strictly tropical plant groups during the Miocene. There is only limited evidence for northward migration of strictly tropical plant lineages in the USA, such as the occurrence of Chrysobalanaceae at Alum Bluff (Lott et al., 2019). By contrast, the evidence for Miocene northward migration of plant groups with distinct subtropical modern-day ranges is much more prevalent, such as *Itea*, *Cyrilla*, *Cleyera*, *Gordonia*, *Persea*, *Symplocos*, *Illicium* and *Melliodendron* recorded in the Brandon Lignite (Tiffney and Barghoorn, 1979; Traverse, 1994; Tiffney et al., 2018). Additionally, the climate of Big Creek was reconstructed as tropical here (Fig. 3b), and its floral composition stands out for its absent temperate floral elements, such as *Carya*, *Pinus* and *Salix* (Supplementary Table S1). It seems therefore that if the climate of, for example, Alum Bluff was truly tropical, 1) the flora would be composed of predominantly tropical plant groups, and 2) there would not be a high number of temperate plant groups mixed in.

4.4.3. *Adaptive radiation*

Paleoclimate reconstructions based on NLRs rely on the assumption that modern-day climatic tolerance of plant groups, constrained by distribution, is representative of the climatic tolerance of the fossil species (Utescher et al., 2014). However, similar to the selective extinction model (Section 4.4.2), modern-day species by definition represent the descendants of those species that were able to adapt, diversify and radiate in response to global climate change that drove others to extinction. Most notably, species that were capable of adapting to cool climates during the Late Miocene and subsequent Plio-Pleistocene cooling (e.g., Westerhold et al., 2020), were able to diversify and radiate, and those descendants make up modern-day vegetation

assemblages. In paleoclimate reconstructions using NLRs, this could result in the paleoclimate envelope only getting defined by the species that radiated and diversified into cooler climates, creating a non-representative bioclimatic envelope (Fig. 8c).

Identifying species-level extinction in plants is notoriously complicated, as is identifying which past species may have been cold tolerant. One approach to this problem is explored in this study (Section 2.2) as species that radiated into cold climates were given less weight. Instead, a diversity-weighted approach is applied here, wherein the climate that the majority of species within a plant group occurs in is more important in defining the optimal climate range for the group. However, this approach still does not account for the potential of diversification events in response to novel climatic niches in Earth's history. In molecular phylogenetic studies, the timing of diversification or adaptive events in groups of organisms can be tested to correlate with the timing of climatic events using ancestral state reconstructions (e.g., Jordan et al., 2008; Manen et al., 2010; Onstein and Linder, 2016). Ancestral state reconstructions could be used in the NLR approach as well, for example by omitting species from the NLR-based reconstruction that are part of a diversification event that postdates the targeted time in Earth's history. However, this approach requires resolving phylogenetic relations at the species level (e.g., Manen et al., 2010) for all plant groups in the fossil assemblage.

4.4.4. Unconstrained control of species distribution

Temperature and precipitation variables have predictive value for species diversity and distribution (Kreft and Jetz, 2014; Iverson et al., 2019). However, the most important abiotic predictors of distribution are highly variable between plant groups and may not always be climatic, but could be edaphic (Iverson et al., 2019). In addition, fire plays an important role in determining vegetation distribution in the eastern USA (Nowacki and Abrams, 2015), with positive feedback mechanisms between vegetation openness and fire recurrence. If the regular occurrence of fire in the Miocene ecosystem is what prevented denser, shade-tolerant vegetation to migrate north, such as rainforest vegetation, then the temperature range suggested by the NLR may not be indicative of the actual temperature (Fig. 8d). Additionally, the effect of high-to-mid-latitude light regimes on mid-to-low-latitude analogue floras has been invoked as a possible confounding factor in plant-based terrestrial paleoclimate studies (e.g., Spicer, 2000; Reichgelt et al., 2015; West et al., 2020).

Edaphic conditions are problematic in NLR analysis, predominantly because soil type preference has strong interspecies variation (e.g., Iverson et al., 2019) and allopatric speciation commonly occurs along edaphic gradients (Kay et al., 2011). Strong interspecies variability in soil type preference may imply that at higher taxonomic levels, such as genus or family, soil type does not play as strong a role in determining distribution. However, the predictive importance of climate and edaphic conditions at the genus- or family-level has not been tested. Testing modern-day distribution patterns of plant genera and families for the relative predictive importance of abiotic factors would elucidate which plant groups are useful for NLR analysis.

Fire recurrence also may be important in determining the distribution of plant groups in the eastern USA. Due to changes in regional climate and anthropogenic suppression of fires in modern time, a process known as “mesophication” is taking place, where fire-prone (pyrophilic) vegetation is replaced with mesophytic forest that typically reduces fire recurrence (pyrophobic, Nowacki and Abrams, 2015). Both may be examples of Alternate Stable State (ASS) vegetation types in which the vegetation type is maintained through positive feedback mechanisms, rather than distinct macroclimate preferences (Nowacki and Abrams, 2008; Pausas and Bond, 2020). In short, pyrophilic vegetation will promote fire through biological and physical adaptations and processes, for example, by maintaining an open, well-lit understory, where ignition and spread of fire is more likely. Pyrophobic vegetation, on the other hand, does the opposite, for example with densely shaded understories, where humidity is high and evaporation reduced, diminishing the likelihood of ignition and spread of fire.

Whether ASS between pyrophobic and pyrophilic vegetation existed in the Miocene is unclear. Only at the Messinian to Zanclean Gray Fossil and Pipe Creek sites has frequent fire disturbance been identified, based on the presence and prevalence of charcoal (Shunk et al., 2009b; Zobaa et al., 2011; Ochoa et al., 2016; Swinehart and Farlow, 2021). However, charcoal abundances were not reported at the other Miocene localities studied here, making a comparison impossible. Nowacki and Abrams (2015) identified the tree genera *Carya*, *Castanea*, *Pinus*, *Populus*, *Quercus* and *Sassafras* as typically pyrophilic in eastern USA forests. The genera identified at the sites studied here (Supplementary Table S1) reveal that none of the sites, including the Gray Fossil and Pipe Creek sites, are exclusively made up of these pyrophilic taxa or have an absence of pyrophobic genera, such as *Acer*, *Fagus*, *Fraxinus*, *Juglans*, *Liquidambar*, *Platanus* or *Ulmus*. However, this does not account for the potential mixing of pyrophilic and pyrophobic vegetation components in fossil assemblages, either because of lateral vegetation mosaics (e.g., riparian and upland vegetation) or short-term vegetation succession. Interestingly, the Brandon Lignite is the only site that lacks pyrophilic vegetation components altogether. Perhaps this indicates a spatial or a temporal trend in the evolution of fire vegetation. However, a more comprehensive investigation of fire indicators, such as charcoal, should be performed in order to examine the changing role of fire in Miocene ecosystems of eastern North America.

4.5. Vegetation heterogeneity

In western North America, the Miocene was characterized by an overall vegetation transition from forests to grasslands (Kukla et al., 2022), as typified by the increasing dominance of C_4-type vegetation (McInerney et al., 2011; Strömberg and McInerney, 2011). Evidence of this vegetation transition in eastern North America is limited, primarily because the climate likely did not favor C_4-type vegetation, or even C_3 grasslands, in the Miocene, but also because of the general sparsity of studied sections. The most comprehensive studies on this topic are again from the Messinian to Zanclean Gray Fossil site and the Pipe Creek sinkhole, where the presence of C_4 vegetation can be established, but the landscape still is dominated by forests (Shunk et al., 2006; DeSantis and Wallace, 2008; Shunk et al., 2009b; Zobaa et al., 2011). The vegetation at the Pipe Creek sinkhole was described as a temperate woodland savanna, with abundant Poaceae (Swinehart and Farlow, 2021) and classified with beech-maple-basswood forest (Ochoa et al., 2016), which agrees with our classification based on FCA (Fig. 6b). A spatial or temporal trend from closed to more open vegetation could not be detected in this study, which agrees with Miocene palynological investigations of the New Jersey hinterland (Kotthoff et al., 2014; Prader et al., 2017, 2020). This suggests that throughout the Miocene, much like today, a mosaic of different wooded biomes existed in the eastern USA.

5. Conclusion

Due to a dearth of sedimentary deposits in the eastern USA, Miocene floras are rare in this region. The available paleofloras span >10° latitude, were deposited at different times, and sometimes have large temporal uncertainties. Creating a continuous record of terrestrial climate and vegetation of the eastern USA is therefore complicated. The available autochthonous paleofloras reveal limited climate variation both spatially and temporally. Mean annual temperature is largely 15–20 °C, and mean annual precipitation 100–150 cm yr^{-1}. Correspondingly, the reconstructed macrobiomes are temperate seasonal forests, similar to those in eastern USA today. The largest deviations relative to today are in the northeast (>35°N) of the USA, where both temperature and precipitation are elevated, suggesting enhanced heat and moisture transport in the globally warmer conditions of the Miocene. Notably, reconstructed Miocene precipitation seasonality is

larger than today. Despite homogeneity in the reconstructed macrobiomes, there was variability in the reconstructed vegetation types. Some Miocene floras clustered confidently with modern vegetation types, specifically subtropical evergreen or beech-maple-basswood forest, although pollen floras could often not be confidently placed. There is no detectable spatial or temporal trend in vegetation type differences.

Reconstructed mean annual temperatures from the eastern USA were cooler than reconstructed coeval North Atlantic average sea surface temperatures from similar latitudes. This may represent the overall higher heat capacity of the ocean in combination with northward heat transport by ocean currents. We highlight the discrepancy between our reconstructed temperatures during the Miocene Climatic Optimum and those derived from a simulation of the Middle Miocene with a new Earth System Model. Plant-based proxies suggest much cooler conditions during the Middle Miocene than the model. Proxy-model discrepancy is reduced when allochthonous plant types are removed, and there is strong proxy-model agreement in reconstructed precipitation. Despite the proxy-model discrepancy, Miocene paleobotanical records allow us to identify regional climatic responses to increased global temperatures that are of importance to the eastern USA in the near future, such as poleward amplification of temperatures and increased precipitation seasonality.

Declaration of Competing Interest

The authors declare no competing interests.

Data availability

The authors have shared the data in the Supplementary Information

Acknowledgements

R.F. acknowledges support from U.S. National Science Foundation grant numbers 1814029. The CESM2 simulations are performed with high-performance computing support from Cheyenne (doi:https://doi.org/10.5065/D6RX99HX) provided by NCAR's Computational and Information Systems Laboratory, sponsored by the National Science Foundation. Upon acceptance of this manuscript, model data used in this study will be uploaded to the public repository Zenodo. A.B. would like to thank Christopher (Yusheng) Liu and the Department of Biological Sciences at East Tennessee State University for support and facilities during her MSc. D.W. was funded by the U.S. Geological Survey Land Change Science/Climate Research & Development Program. Any use of trade, firm, or product names is for descriptive purposes only and does not imply endorsement by the U.S. Government. We would like to thank Robert Poirier and Marci Robinson at USGS for their insightful preliminary reviews of the manuscript, as well as Torsten Utescher and an anonymous reviewer for their constructive reviews.

Appendix A. Supplementary data

Supplementary data to this article can be found online at https://doi.org/10.1016/j.gloplacha.2023.104073.

References

Allstädt, F.J., Koutsondendris, A., Appel, E., Rösler, W., Reichgelt, T., Kaboth-Bar, S., Prokopenko, A.A., Pross, J., 2021. Late Pliocene to early Pleistocene climate dynamics in western North America based on a new pollen record from paleo-Lake Idaho. Palaeobiodivers. Palaeoenviron. 101, 177–195.

Anderson-Teixeira, K.J., Davies, S.J., Bennett, A.C., Gonzalez-Akre, E.B., Muller-Landau, H.C., Joseph Wright, S., Abu Salim, K., Almeyda Zambrano, A.M., Alonso, A., Baltzer, J.L., Basset, Y., Bourg, N.A., Broadbent, E.N., Brockelman, W.Y., Bunyavejchewin, S., Burslem, D.F.R.P., Butt, N., Cao, M., Cardenas, D., Chuyong, G. B., Clay, K., Cordell, S., Dattaraja, H.S., Deng, X., Detto, M., Du, X., Duque, A., Erikson, D.L., Ewango, C.E.N., Fischer, G.A., Fletcher, C., Foster, R.B., Giardina, C.P., Gilbert, G.S., Gunatilleke, N., Gunatilleke, S., Hao, Z., Hargrove, W.W., Hart, T.B., Hau, B.C.H., He, F., Hoffman, F.M., Howe, R.W., Hubbell, S.P., Inman-Narahari, F. M., Jansen, P.A., Jiang, M., Johnson, D.J., Kanzaki, M., Kassim, A.R., Kenfack, D., Kibet, S., Kinnaird, M.F., Korte, L., Kral, K., Kumar, J., Larson, A.J., Li, Y., Li, X., Liu, S., Lum, S.K.Y., Lutz, J.A., Ma, K., Maddalena, D.M., Makana, J.-R., Malhi, Y., Marthews, T., Mat Serudin, R., McMahon, S.M., McShea, W.J., Memiaghe, H.R., Mi, X., Mizuno, T., Morecroft, M., Myers, J.A., Novotny, V., de Oliveira, A.A., Ong, P. S., Orwig, D.A., Ostertag, R., den Ouden, J., Parker, G.G., Phillips, R.P., Sack, L., Sainge, M.N., Sang, W., Sri-ngernyuang, K., Sukumar, R., Sun, I.-F., Sungpalee, W., Suresh, H.S., Tan, S., Thomas, S.C., Thomas, D.W., Thompson, J., Turner, B.L., Uriarte, M., Valencia, R., Vallejo, M.I., Vicentini, A., Vrška, T., Wang, X., Wang, X., Weiblen, G., Wolf, A., Xu, H., Yap, S., Zimmerman, J., 2015. CTFS-ForestGEO: a worldwide network monitoring forests in an era of global change. Glob. Chang. Biol. 21, 528–549.

Beck, H.E., Zimmerman, N.E., McVicar, T.R., Vergopolan, N., Berg, A., Wood, E.F., 2018. Present and future Köppen-Geiger climate classification maps at 1-km resolution. Scientific Data 5, 180214.

Bekryaev, R.V., Polyakov, I.V., Alexeev, V.A., 2010. Role of polar amplification in long-term surface are temperature variations and modern Arctic warming. J. Clim. 23, 3888–3906.

Benson, R.N., 1998. Radiolarians and diatoms from the Pollack Farm Site, Delaware: Marine–Terrestrial correlation of Miocene vertebrate assemblages of the Middle Atlantic Coastal Plain. In: Benson, R.N. (Ed.), Geology and Paleontology of the Lower Miocene Pollack Farm Fossil Site, Delaware. Delaware Geological Survey Special Publication, Newark, Delaware, pp. 5–20.

Berry, E.W., 1916. The flora of the Catahoula sandstone. In: USGS Professional Paper 98-M, pp. 227–251.

Böhme, M., Ilg, A., Winklhofer, M., 2008. Late Miocene "washhouse" climate in Europe. Earth Planet. Sci. Lett. 275, 393–401.

Brenner, G.J., Sugarman, P.J., Miller, K.G., 1997. 20. Data report: Miocene palynologic and climatic records, New Jersey coastal plain. In: Miller, K.G., Snyder, S.W. (Eds.), Proceedings of the Ocean Drilling Program. Scientific Results. Ocean Drilling Program, College Station, TX, pp. 277–285.

Burls, N.J., Bradshaw, C.D., De Boer, A.M., Herold, N., Huber, M., Pound, M.J., Donnadieu, Y., Farnsworth, A., Frigola, A., Gasson, E., von der Heydt, A.S., Hutchinson, D.K., Knorr, G., Lawrence, K.T., Lear, C.H., Li, X., Lohmann, G., Lunt, D. J., Marzocchi, A., Prange, M., Riihimaki, C.A., Sarr, A.-C., Siler, N., Zhang, Z., 2021. Simulating Miocene warmth: insights from an opportunistic multi-model ensemble (MioMIP1). Paleoceanography Paleoclimatol. 36 e2020PA004054.

Carmichael, M.J., Lunt, D.J., Huber, M., Heinemann, M., Kiehl, J.T., LeGrande, A., Loptson, C.A., Roberts, C.D., Sagoo, N., Shields, C.A., Valdes, P.J., Winguth, A., Winguth, C., Pancost, R.D., 2016. A model–model and data–model comparison for the early Eocene hydrological cycle. Clim. Past 12, 455–481.

Carter, L., Dow, K., Hiers, K., Kunkel, K.E., Lascurain, A., Marcy, D., Osland, M., Schramm, P., 2018. Southeast. In: Reidmiller, D.R., Avery, C.W., Easterling, D.R., Kunkel, K.E., Lewis, K.L.M., Maycock, T.K., Stewart, B.C. (Eds.), Impacts, Risks, and Adaptation in the United States: Fourth National Climate Assessment. U.S. Global Change Research Program, Washington D.C., pp. 743–808

Chevalier, M., Davis, B.A.S., Heiri, O., Seppä, H., Chase, B.M., Gajewski, K., Lacourse, T., Telford, R.J., Finsinger, W., Guiot, J., Kühl, N., Maezumi, S.Y., Tipton, J.R., Carter, V.A., Brussel, T., Phelps, L., Dawson, A., Zanon, M., Vallé, F., Nolan, C., Mauri, A., de Vernal, A., Izumi, K., Holmström, L., Marsicek, J., Goring, S., Sommer, P.S., Chaput, M., Kupriyanov, D., 2020. Pollen-based climate reconstruction techniques for late Quaternary studies. Earth Sci. Rev. 210, 103384.

Danabasoglu, G., Lamarque, J.-F., Bacmeister, J., Bailey, D.A., DuVivier, A.K., Edwards, J., Emmons, L.K., Fasullo, J., Garcia, R., Gettelman, A., Hannay, C., Holland, M.M., Large, W.G., Lauritzen, P.H., Lawrence, D.M., Lenaerts, J.T.M., Lindsay, K., Lipscomb, W.H., Mills, M.J., Neale, R., Oleson, K.W., Otto-Bliesner, B.L., Phillips, A.S., Sacks, W., Tilmes, S., van Kampenhout, L., Vertenstein, M., Bertini, A., Dennis, J., Deser, C., Fischer, C., Fox-Kemper, B., Kay, J.E., Kinnison, D., Kushner, P. J., Larson, V.E., Long, M.C., Mickelson, S., Moore, J.K., Nienhouse, E., Polvani, L., Rasch, P.J., Strand, W.G., 2020. The community earth system model version 2 (CESM2). J. Adv. Model. Earth Syst. 12 e2019MS001916.

De Cáceres, M., Font, X., Oliva, F., 2010. The management of vegetation classifications with fuzzy clustering. J. Veg. Sci. 21, 1138–1151.

DeSantis, L.R.G., Wallace, S.C., 2008. Neogene forests from the Appalachians of Tennessee, USA: Geochemical evidence from fossil mammal teeth. Palaeogeogr. Palaeoclimatol. Palaeoecol. 266, 59–68.

Dupigny-Giroux, L.-A.L., Lemcke-Stampone, M.D., Hodgkins, G.A., Lentz, E.E., Mills, K. E., Lane, E.D., Miller, R., Hollinger, D.Y., Solecki, W.D., Wellenius, G.A., Sheffield, P. E., MacDonald, A.B., Caldwell, C., 2018. Northeast. In: Reidmiller, D.R., Avery, C.W., Easterling, D.R., Kunkel, K.E., Lewis, K.L.M., Maycock, T.K., Stewart, B.C. (Eds.), Impacts, Risks, and Adaptation in the United States: Fourth National Climate Assessment. U.S. Global Change Research Program, Washington DC, pp. 669–742.

Dyer, J.M., 2006. Revisiting the deciduous forests of eastern North America. BioScience 56, 341–352.

Easterling, D.R., Kunkel, K.E., Arnold, J.R., Knutson, T., LeGrande, A.N., Leung, L.R., Vose, R.S., Waliser, D.E., Wehner, M.F., 2017. Precipitation change in the Unites States. In: Wuebbles, D.J., Fahey, D.W., Hibbard, K.A., Dokken, D.J., Steward, Maycock, T.K. (Eds.), Climate Science Special Report: Fourth National Climate Assessment. U.S. Global Change Research Program, Washington D.C., pp. 207–230

Farlow, J.O., Sunderman, J.A., Havens, J.J., Swinehart, A.L., Holman, A.J., Richards, R. L., Miller, N.G., Martin, R.A., Hunt, R.M., Storrs, G.W., Curry, B.B., Fluegeman, R.H., Dawson, M.R., Flint, M.E.T., 2001. The Pipe Creek Sinkhole biota, a diverse late Tertiary continental fossil assemblage from Grant County, Indiana. Am. Midl. Nat. 145, 367–378.

Feng, R., Otto-Bliesner, B.L., Brady, E.C., Rosenbloom, N., 2020. Increased climate response and Earth System Sensitivity from CCSM4 to CESM2 in mid-Pliocene simulations. J. Adv. Model. Earth Syst. 12 e2019MS002033.
Ferguson, D.K., 1985. The origin of leaf-assemblages – new light on an old problem. Rev. Palaeobot. Palynol. 46, 117–188.
Foster, G.L., Royer, D.L., Lunt, D.J., 2017. Future climate focing potentially without precedent in the last 420 million years. Nat. Commun. 8, 14845.
Frederiksen, N.O., 1984. Stratigraphic, paleoclimatic, and paleobiogeographic significance of Tertiary sporomorphs from Massachusetts. In: USGS Professional Paper, 1308, p. 25.
Frigola, A., Prange, M., Schultz, M., 2018. Boundary conditions for the Middle Miocene climate transition (MMCT v1.0). Geosci. Model Dev. 11, 1607–1626.
GBIF.org, 2021. GBIF Home Page. Available from: https://www.gbif.org.
Godfrey, C., Fan, M., Jesmok, G., Upadhyay, D., Tripati, A., 2018. Petrography and stable isotope geochemistry of Oligocene-Miocene continental carbonates in South Texas: Implications for paleoclimate and paleoenvironment near sea-level. Sediment. Geol. 367, 69–83.
Goldner, A., Herold, N., Huber, M., 2014. The challenge of simulating the warmth of the mid-Miocene climatic optimum in CESM1. Clim. Past 10, 523–536.
Gong, F., Karsai, I., Liu, Y.-S., 2010. *Vitis* seeds (Vitaceae) from the late Neogene Gray Fossil Site, northeastern Tennessee, U.S.a. Rev. Palaeobot. Palynol. 162, 71–83.
Greller, A.M., Rachele, L.D., 1983. Climatic limits of exotic genera in the Legler palynoflora, Miocene, New Jersey, U.S.a. Rev. Palaeobot. Palynol. 40, 149–163.
Grimm, G.W., Potts, A.J., 2016. Fallacies and fantasies: the theoretical underpinnings of the Coexistence Approach for palaeoclimate reconstruction. Clim. Past 12, 611–622.
Grimm, G.W., Bouchal, J.M., Denk, T., Potts, A., 2016. Fables and foibles: a critical analysis of the Palaeoflora database and the Coexistence Approach for palaeoclimate reconstruction. Rev. Palaeobot. Palynol. 233, 216–235.
Groot, J.J., 1998. Palynomorphs from the lower Miocene Pollack Farm site, Delaware. In: Benson, R.N. (Ed.), Geology and Paleontology of the Lower Miocene Pollack Farm Fossil Site, Delaware. Delaware Geological Survey Special Publication, Newark, Delaware, pp. 55–57.
Guitián, J., Phelps, S.R., Polissar, P.J., Ausín, B., Eglinton, T.I., Stoll, H.M., 2019. Midlatitude temperature variations in the Oligocene to early Miocene. Paleoceanography Paleoclimatol. 34, 1328–1343.
Herbert, T.D., Lawrence, K.T., Tzanova, A., Peterson, L.C., Caballero-Gill, R., Kelly, C.S., 2016. Late Miocene global cooling and the rise of modern ecosystems. Nat. Geosci. 9, 843–847.
Hermsen, E.J., 2021. Review of the fossil record of Passiflora, with a description of new seeds from the Pliocene Gray Fossil Site, Tennessee, USA. Int. J. Plant Sci. 182, 533–550.
Herold, N., Seton, M., Müller, R.D., You, Y., Huber, M., 2008. Middle Miocene tectonic boundary conditions for use in climate models. Geochem. Geophys. Geosyst. 9, 10.
Herold, N., Müller, R.D., Seton, M., 2010. Comparing early to Middle Miocene terrestrial climate simulations with geological data. Geosphere 6, 952–961.
Hijmans, R.J., Phillips, S., Leathwick, J., Elith, J., 2017. dismo: Species Distribution Modeling. R package version 1, pp. 1–4. https://CRAN.R-project.org/package=dismo.
Hollis, C.J., Dunkley Jones, T., Anagnostou, E., Bijl, P.K., Cramwinckel, M.J., Cui, Y., Dickens, G.R., Edgar, K.M., Eley, Y., Evans, D., Foster, G.L., Frieling, J., Inglis, G.N., Kennedy, E.M., Kozdon, R., Lauretano, V., Lear, C.H., Littler, K., Lourens, L., Meckler, A.N., Naafs, B.D.A., Pälike, H., Pancost, R.D., Pearson, P.N., Röhl, U., Royer, D.L., Salzmann, U., Schubert, B.A., Seebeck, H., Sluijs, A., Speijer, R.P., Stassen, P., Tierney, J., Tripati, A., Wade, B., Westerhold, T., Witkowski, C., Zachos, J.C., Zhang, Y.G., Huber, M., Lunt, D.J., 2019. The DeepMIP contribution to PMIP4: methodologies for selection, compilation and analysis of latest Paleocene and early Eocene climate proxy data, incorporating version 0.1 of the DeepMIP database. Geosci. Model Dev. 12, 3149–3206.
Huang, Y., Liu, Y.-S., Zavada, M., 2014. New fossil fruits of *Carya* (Juglandaceae) from the latest Miocene to earliest Pliocene in Tennessee, eastern United States. J. Syst. Evol. 52, 508–520.
Huang, Y., Liu, Y.-S., Wen, J., Quan, C., 2015. First fossil record of *Staphylea* L. (Staphyleaceae) from North America, and its biogeographic implications. Plant Syst. Evol. 301, 2203–2218.
Hurrell, J.W., Hack, J.J., Shea, D., Caron, J.M., Rosinski, J., 2008. A new sea surface temperature and sea ice boundary dataset for the community atmosphere model. J. Clim. 21, 5145–5153.
Hutchinson, D.K., Coxall, H.K., Lunt, D.J., Steinthorsdottir, M., de Boer, A.M., Baatsen, M., von der Heydt, A.S., Huber, M., Kennedy-Asser, A.T., Kunzmann, L., Ladant, J.-B., Lear, C.H., Moraweck, K., Pearson, P.N., Piga, E., Pound, M.J., Salzmann, U., Scher, H.D., Sijp, W.P., Śliwińska, K.K., Wilson, P.A., Zhang, Z., 2021. The Eocene–Oligocene transition: a review of marine and terrestrial proxy data, models and model–data comparisons. Clim. Past 17, 269–315.
Huurdeman, E.P., Frieling, J., Reichgelt, T., Bijl, P.K., Bohaty, S.M., Holdgate, G.R., Gallagher, S.J., Peterse, F., Greenwood, D.R., Pross, J., 2021. Rapid expansion of meso-megathermal rain forests into the southern high latitudes at the onset of the Paleocene-Eocene thermal Maximum. Geology 49, 40–44.
Hyland, E.G., Huntington, K.W., Sheldon, N.D., Reichgelt, T., 2018. Temperature seasonality in the north American continental interior during the early Eocene Climatic Optimum. Clim. Past 14, 1391–1404.
Isphording, W.C., 1970. Late Tertiary paleoclimate of eastern United States. Am. Assoc. Pet. Geol. Bull. 54, 334–343.
Ivanov, D., Utescher, T., Mosbrugger, V., Syabryaj, S., Djordjević-Milutinović, D., Molchanoff, S., 2011. Miocene vegetation and climate dynamics in Eastern and Central Paratethys (Southeastern Europe). Palaeogeogr. Palaeoclimatol. Palaeoecol. 304, 262–275.
Iverson, L.R., Prasad, A.M., Matthews, S.N., Peters, M., 2008. Estimating potential habitat for 134 eastern US tree species under six climate scenarios. For. Ecol. Manag. 254, 390–406.
Iverson, L.R., Peters, M.P., Prasad, A.M., Matthews, S.N., 2019. Analysis of climate change impacts on tree species of eastern US: results of DISTRIB-II modeling. Forests 10, 302.
Jackson, S.T., Williams, J.W., 2004. Modern analogs in Quaternary paleoecology: Here today, gone yesterday, gone tomorrow? Annu. Rev. Earth Planet. Sci. 32, 495–537.
Janis, C.M., Damuth, J., Theodor, J.M., 2004. The species richness of Miocene browsers, and implications for habitat type and primary productivity in the north American grassland biome. Palaeogeogr. Palaeoclimatol. Palaeoecol. 207, 371–398.
Jarzen, D.M., Corbett, S.L., Manchester, S.R., 2010. Palynology and paleoecology of the Middle Miocene Alum Bluff flora, Liberty County, Florida, USA. Palynology 34, 261–286.
Jones, D.S., Ward, L.W., Mueller, P.A., Hodell, D.A., 1998. Age of marine mollusks from the lower Miocene Pollack Farm site, Delaware. In: Benson, R.N. (Ed.), Geology and Paleontology of the Lower Miocene Pollack Farm Fossil Site, Delaware. Delaware Geological Survey Special Publication, Newark, Delaware, pp. 21–26.
Jordan, G.J., Weston, P.H., Carpenter, R.J., Dillon, R.A., Brodribb, T.J., 2008. The evolutionary relations of sunken, covered, and encrypted stomata to dry habitats in Proteaceae. Am. J. Bot. 95, 521–530.
Kay, K.M., Ward, K.L., Watt, L.R., Schemske, D.W., 2011. Plant speciation. In: Harrison, S.P., Rajakaruna, N. (Eds.), Serpentine: The Evolution and Ecology of a Model System. University of California Press, Oakland, California, pp. 71–95.
Kiehl, J.T., Zarzycki, C.M., Shields, C.A., Rothstein, M.V., 2021. Simulated changes to tropical cyclones across the Paleocene-Eocene thermal Maximum (PETM) boundary. Palaeogeogr. Palaeoclimatol. Palaeoecol. 572, 110421.
Knutson, T.R., Sirutis, J.J., Zhao, M., Tuleya, R.E., Bender, M., Vecchi, G.A., Villarini, G., Chavas, D., 2015. Global projections of intense tropical cyclone activity for the late twenty-first century from dynamical downscaling of CMIP5/RCP4.5 scenarios. J. Clim. 28, 7203–7224.
Kotthoff, U., Greenwood, D.R., McCarthy, F.M.G., Müller-Navarra, K., Prader, S., Hesselbo, S.P., 2014. Late Eocene to Middle Miocene (33 to 13 million years ago) vegetation and climate development on the north American Atlantic Coastal Plain (IODP Expedition 313, Site M0027). Clim. Past 10, 1523–1539.
Kreft, H., Jetz, W., 2014. Global patterns and determinants of vascular plant diversity. PNAS 104, 5925–5930.
Kukla, T., Rugenstein, J.K.C., Ibarra, D.E., Winnick, M.J., Strömberg, C.A.E., Chamberlain, C.P., 2022. Drier winters drove Cenozoic open habitat expansion in North America. AGU Adv. 3 e2021AV000566.
Kürschner, W.M., Kvaček, Z., Dilcher, D.L., 2008. The impact of Miocene atmospheric carbon dioxide fluctuations on climate and the evolution of terrestrial ecosystems. PNAS 105, 449–453.
Kvaček, Z., Teodoridis, V., Mach, K., Přikryl, T., Dvořák, Z., 2014. Tracing the Eocene-Oligocene transition: a case study from North Bohemia. Bull. Geosci. 89, 21–65.
Levin, E.L., Murakami, H., 2019. Impact of Anthropogenic climate change on United States major hurricane landfall frequency. J. Mar. Sci. Eng. 7, 135.
Liu, Y.-S., Jacques, F.M.B., 2010. *Sinomenium macrocarpum* sp. nov. (Menispermaceae) from the Miocene–Pliocene transition of Gray, northeast Tennessee, USA. Rev. Palaeobot. Palynol. 159, 112–122.
Lott, T.A., Manchester, S.R., Corbett, S.L., 2019. The Miocene flora of Alum Bluff, Liberty County, Florida. Acta Palaeobotanica 59, 75–129.
Lowe, A.J., Greenwood, D.R., West, C.K., Galloway, J.M., Sudermann, M., Reichgelt, T., 2018. Plant community ecology and climate on an upland volcanic landscape during the early Eocene Climatic Optimum: McAbee Fossil Beds, British Columbia, Canada. Palaeogeogr. Palaeoclimatol. Palaeoecol. 511, 433–448.
Mander, L., Punyasena, S.W., 2018. Fossil pollen and spores in paleoecology. In: Croft, D., Su, D., Simpson, S. (Eds.), Methods in Paleoecology. Vertebrate Paleobiology and Paleoanthropology, Springer, Cham, pp. 215–234.
Manen, J.-F., Barriera, G., Loizeau, P.-A., Naciri, Y., 2010. The history of extant *Ilex* species (Aquifoliaceae): evidence of hybridization within a Miocene radiation. Mol. Phylogenet. Evol. 57, 961–977.
McCartan, L., Tiffney, B.H., Wolfe, J.A., Ager, T.A., Wing, S.L., Sirkin, L.A., Ward, L.W., Brooks, J., 1990. Late Tertiary floral assemblage from upland gravel deposits of the southern Maryland Coastal Plain. Geology 18, 311–314.
McGlone, M.S., Mildenhall, D.C., Pole, M.S., 1996. History and paleoecology of New Zealand *Nothofagus* forests. In: Veblen, T.T., Hill, R.S., Reid, J. (Eds.), The Ecology and Biogeography of *Nothofagus* Forests. Yale University Press, pp. 83–130.
McInerney, F.A., Strömberg, C.A.E., White, J.W.C., 2011. The Neogene transition from C_3 to C_4 grasslands in North America: stable carbon isotope ratios of fossil phytoliths. Paleobiology 37, 23–49.
McNair, D.M., Stults, D.Z., Axsmith, B.J., Alford, M.H., Starnes, J.E., 2019. Preliminary investigation of a diverse megafossil floral assemblage from the Middle Miocene of southern Mississippi, USA. Palaeontol. Electron. 22.2.40A, 1–30.
Methner, K., Campani, M., Fiebig, J., Löffler, N., Kempf, O., Mulch, A., 2020. Middle Miocene long-term continental temperature change in and out of pace with marine climate records. Sci. Rep. 10, 7989.
Micheels, A., Bruch, A.A., Eronen, J.T., Fortelius, M., Harzhauser, M., Utescher, T., Mosbrugger, V., 2011. Analysis of heat transport mechanisms from a late Miocene model experiment with a fully-coupled atmosphere-ocean general circulation model. Palaeogeogr. Palaeoclimatol. Palaeoecol. 304, 337–350.
Mildenhall, D.C., Kennedy, E.M., Lee, D.E., Kaulfuss, U., Bannister, J.M., Fox, B.R.S., Conran, J.G., 2014. Palynology of the early Miocene Foulden Maar, Otago, New Zealand: Diversity following destruction. Rev. Palaeobot. Palynol. 204, 27–42.
Moraweck, K., Uhl, D., Kunzmann, L., 2015. Estimation of late Eocene (Bartonian–Priabonian) terrestrial palaeoclimate: Contributions from megafloral

assemblages from Central Germany. Palaeogeogr. Palaeoclimatol. Palaeoecol. 433, 247–258.
Müller, R.D., Cannon, J.S., Qin, X., Watson, R.J., Gurnis, M., Williams, S., Pfaffelmoser, T., Seton, M., Russell, S.H.J., Zahirovic, S., 2018. GPlates: Building a virtual Earth through deep time. Geochem. Geophys. Geosyst. 19, 2243–2261.
Ning, L., Bradley, R.S., 2015. Snow occurrence changes over the central and eastern United States under future warming scenarios. Sci. Rep. 5, 17073.
Nowacki, G.J., Abrams, M.D., 2008. The demise of fire and "mesophication" of forests in the eastern United States. BioScience 58, 123–138.
Nowacki, G.J., Abrams, M.D., 2015. Is climate an important driver of post-European vegetation change in the eastern United States. Glob. Chang. Biol. 21, 314–334.
Ochoa, D., Whitelaw, M., Liu, Y.-S., Zavada, M., 2012. Palynology of Neogene sediments at the Gray Fossil Site, Tennessee, USA: Floristic implications. Rev. Palaeobot. Palynol. 184, 36–48.
Ochoa, D., Zavada, M.S., Liu, Y.-S., Farlow, J.O., 2016. Floristic implications of two contemporaneous inland upper Neogene sites in the eastern US: Pipe Creek Sinkhole, Indiana, and the Gray Fossil Site, Tennessee (USA). Palaeobiodivers. Palaeoenviron. 96, 239–254.
O'Gorman, P.A., 2014. Contrasting responses of mean and extreme snowfall to climate change. Nature 512, 416–418.
Onstein, R.E., Linder, H.P., 2016. Beyond climate: convergence in fast evolving sclerophylls in Cape and Australian Rhamnaceae predates the mediterranean climate. J. Ecol. 104, 665–677.
Pausas, J.G., Bond, W.J., 2020. Alternative biome states in terrestrial ecosystems. Trends Plant Sci. 25, 250–263.
Pazzaglia, F.J., Robinson, R.A.J., Traverse, A., 1997. Palynology of the Bryn Mawr Formation (Miocene): insights on the age and genesis of Middle Atlantic margin fluvial deposits. Sediment. Geol. 108, 19–44.
Peppe, D.J., Baumgartner, A., Flynn, A., Blonder, B., 2018. Reconstructing paleoclimate and paleoecology using fossil leaves. In: Croft, D.A., Su, D., Simpson, S.W. (Eds.), Methods in Paleoecology. Vertebrate Paleobiology and Paleoanthropology, Springer, Cham, pp. 289–317.
Peterse, F., van der Meer, J., Schouten, S., Weijers, J.W.H., Fierer, N., Jackson, R.B., Kim, J.-H., Sinninghe Damsté, J.S., 2012. Revised calibration of the MBT–CBT paleotemperature proxy based on branched tetraether membrane lipids in surface soils. Geochim. Cosmochim. Acta 96, 215–229.
Peterson, T.C., Heim Jr., R.R., Hirsch, R., Kaiser, D.P., Brooks, H., Diffenbauch, N.S., Dole, R.M., Giovannettone, J.P., Guirguis, K., Karl, T.R., Katz, R.W., Kunkel, K.E., Lettenmaier, D., McCabe, G.J., Paciorek, C.J., Ryberg, K.R., Schubert, S., Silva, V.B. S., Stewart, B.C., Vecchia, A.V., Villarini, G., Vose, R.S., Walsh, J., Wehner, M., Wolock, D., Wolter, K., Woodhouse, C.A., Wuebbles, D.J., 2013. Monitoring and understanding changes in heat waves, cold waves, floods, and droughts in the United States. Bull. Am. Meteorol. Soc. 94, 821–834.
Pound, M.J., Haywood, A.M., Salzmann, U., Riding, J.B., 2012. Global vegetation dynamics and latitudinal temperature gradients during the Mid to late Miocene (15.97–5.33 Ma). Earth Sci. Rev. 112, 1–22.
Prader, S., Kotthoff, U., McCarthy, F.M.G., Schmiedl, G., Donders, T.H., Greenwood, D. R., 2017. Vegetation and climate development of the New Jersey hinterland during the late Middle Miocene (IODP Expedition 313 Site M0027). Palaeogeogr. Palaeoclimatol. Palaeoecol. 485, 854–868.
Prader, S., Kotthoff, U., Greenwood, D.R., McCarthy, F.M.G., Schmiedl, G., Donders, T. H., 2020. New Jersey's paleoflora and eastern North American climate through Paleogene–Neogene warm phases. Rev. Palaeobot. Palynol. 279, 104224.
Prentice, I.C., Farquhar, G.D., Fasham, M.J.R., Goulden, M.L., Heimann, M., Jaramillo, V. J., Kheshgi, H.S., Le Quéré, C., Scholes, R.J., Wallace, D.W.R., 2001. The carbon cycle and atmospheric carbon dioxide. In: Houghton, J.T., Ding, Y., Griggs, D.J., Noguer, M., van der Linden, P.J., Xiaosu, D. (Eds.), Climate Change 2001: The Scientific Basis. Cambridge University Press, Cambridge UK, p. 56.
Pross, J., Contreras, L., Bijl, P.K., Greenwood, D.R., Bohaty, S.M., Schouten, S., Bendle, J. A., Röhl, U., Tauxe, L., Raine, J.I., Huck, C.E., van de Flierdt, T., Jamieson, S.S.R., Stickley, C.E., Van de Schootbrugge, B., Escutia, C., Brinkhuis, H., 2012. Persistent near-tropical warmth on the Antarctic continent during the early Eocene epoch. Nature 48, 73–77.
Quirk, Z.J., Hermsen, E.J., 2021. Neogene Corylopsis seeds from eastern Tennessee. J. Syst. Evol. 59, 611–621.
R Core Team, 2021. R: A Language and Environment for Statistical Computing. R Foundation for Statistical Computing, Vienna, Austria. https://www.R-project.org/.
Rachele, L.D., 1976. Palynology of the Legler Lignite: a deposit in the Tertiary Cohansey Formation of New Jersey, U.S.a. Rev. Palaeobot. Palynol. 22, 225–252.
Rech, A.R., Dalsgaard, B., Sandel, B., Sonne, J., Svenning, J.-C., Holmes, N., Ollerton, J., 2016. The macroecology of animal versus wind pollination: ecological factors are more important than historical climate stability. Plant Ecol. Divers. 9, 253–262.
Regal, P.J., 1982. Pollination by wind and animals: ecology of geographic patterns. Annu. Rev. Ecol. Syst. 13, 497–524.
Reichgelt, T., Kennedy, E.M., Conran, J.G., Mildenhall, D.C., Lee, D.E., 2015. The early Miocene paleolake Manuherikia: vegetation heterogeneity and warm-temperate to subtropical climate in southern New Zealand. J. Paleolimnol. 53, 349–365.
Reichgelt, T., West, C.K., Greenwood, D.R., 2018. The relation between global palm distribution and climate. Sci. Rep. 8, 4721.
Reichgelt, T., D'Andrea, W.J., Valdivia-McCarthy, A.D.C., Fox, B.R.S., Bannister, J.M., Conran, J.G., Lee, W.G., Lee, D.E., 2020. Elevated CO_2, increased leaf-level productivity, and water-use efficiency during the early Miocene. Clim. Past 16, 1509–1521.
Reichgelt, T., Greenwood, D.R., Steinig, S., Conran, J.G., Hutchinson, D.K., Lunt, D.J., Scriven, L.J., Zhu, J., 2022. Plant proxy evidence for high rainfall and productivity in the Eocene of Australia. Paleoceanography Paleoclimatol. 37 e2022PA004418.
Rich, F.J., Pirkle, F.L., Arenberg, E., 2002. Palynology and paleoecology of strata associated with the Ohoopee river dune field, Emanuel county, Georgia. Palynology 26, 239–256.
Rubel, F., Kottek, M., 2010. Observed and projected climate shifts 1901–2100 depicted by world maps of the Köppen-Geiger climate classification. Meteorol. Z. 19, 135–141.
Rubel, F., Brugger, K., Haslinger, K., Auer, I., 2017. The climate of the European Alps: Shift of very high resolution Köppen-Geiger climate zones 1800–2100. Meteorol. Z. 26, 115–125.
Samuels, J.X., Bredehoeft, K.E.W., Steven, C., 2018. A new species of *Gulo* from the early Pliocene Gray Fossil Site (Eastern United States); rethinking the evolution of wolverines. PeerJ 6, e4648.
Shukla, A., Mehrotra, R.C., Spicer, R.A., Spicer, T.E.V., Kumar, M., 2014. Cool equatorial terrestrial temperatures and the south Asian monsoon in the early Eocene: evidence from the Gurha Mine, Rajasthan, India. Palaeogeogr. Palaeoclimatol. Palaeoecol. 412, 187–198.
Shunk, A.J., Driese, S.G., Clark, G.M., 2006. Latest Miocene to earliest Pliocene sedimentation and climate record derived from paleosinkhole fill deposits, Gray Fossil Site, northeastern Tennessee, U.S.a. Palaeogeogr. Palaeoclimatol. Palaeoecol. 231, 265–278.
Shunk, A.J., Driese, S.G., Dunbar, J.A., 2009a. Late Tertiary paleoclimate interpretation from lacustrine rhythmites in the Gray Fossil Site, northeastern Tennessee, USA. J. Paleolimnol. 42, 11–24.
Shunk, A.J., Driese, S.G., Farlow, J.O., Zavada, M.S., Zobaa, M.K., 2009b. Late Neogene paleoclimate and paleoenvironment reconstructions from the Pipe Creek Sinkhole, Indiana, USA. Palaeogeogr. Palaeoclimatol. Palaeoecol. 274, 173–184.
Smith, D.M., Screen, J.A., Deser, C., Cohen, J., Fyfe, J.C., García-Serrano, J., Jung, T., Kattsov, V., Matei, D., Msadek, R., Peings, Y., Sigmond, M., Ukita, J., Yoon, J.-H., Zhang, X., 2019. The Polar Amplification Model Intercomparison Project (PAMIP) contribution to CMIP6: investigating the causes and consequences of polar amplification. Geosci. Model Dev. 12, 1139–1164.
Sosdian, S.M., Greenop, R., Hain, M.P., Foster, G.L., Pearson, P.N., Lear, C.H., 2018. Constraining the evolution of Neogene Ocean carbonate chemistry using the boron isotope pH proxy. Earth Planet. Sci. Lett. 498, 362–376.
Spicer, R.A., 1989. The formation and interpretation of plant fossil assemblages. Adv. Bot. Res. 16, 95–191.
Spicer, R.A., 2000. Leaf physiognomy and climate change. In: Culver, S.J., Rawson, P.F. (Eds.), Biotic Response to Global Change: The Last 145 Million Years. Cambridge University Press, Cambridge, pp. 244–264.
Spicer, R.A., Herman, A.B., Liao, W., Spicer, T.E.V., Kodrul, T.M., Yang, J., Jin, J., 2014. Cool tropics in the Middle Eocene: evidence from the Changchang Flora, Hainan Island, China. Palaeogeogr. Palaeoclimatol. Palaeoecol. 412, 1–16.
Spicer, R.A., Yang, J., Spicer, T.E.V., Farnsworth, A., 2020. Woody dicot leaf traits as a palaeoclimate proxy: 100 years of development and application. Palaeogeogr. Palaeoclimatol. Palaeoecol. 562, 110138.
Steinthorsdottir, M., Coxall, H.K., de Boer, A.M., Huber, M., Barbolini, N., Bradshaw, C. D., Burls, N.J., Feakins, S.J., Gasson, E., Henderiks, J., Holbourn, A.E., Kiel, S., Kohn, M.J., Knorr, G., Kürschner, W.M., Lear, C.H., Liebrand, D., Lunt, D.J., Mörs, T., Pearson, P.N., Pound, M.J., Stoll, H.M., Strömberg, C.A.E., 2021. The Miocene: the future of the past. Paleoceanography Paleoclimatol. 36 e2020PA004037.
Strömberg, C.A.E., McInerney, F.A., 2011. The Neogene transition from C_3 to C_4 grasslands in North America: assemblage analysis of fossil phytoliths. Paleobiology 37, 50–71.
Super, J.R., Thomas, E., Pagani, M., Huber, M., O'Brien, C., Hull, P.M., 2018. North Atlantic temperature and pCO_2 coupling in the Early-Middle Miocene. Geology 46, 519–522.
Swinehart, A.L., Farlow, J.O., 2021. Plant and invertebrate macrofossils from the Pipe Creek Sinkhole (late Neogene), Grant County, Indiana. Hist. Biol. 33, 3111–3140.
Thompson, N., Salzmann, U., López-Quirós, A., Bijl, P.K., Hoem, F.S., Etourneau, J., Sicre, M.-A., Roignant, S., Hocking, E., Amoo, M., Escutia, C., 2022. Vegetation change across the Drake Passage region linked to Late Eocene cooling and glacial disturbance after the Eocene–Oligocene transition. Clim. Past 18, 209–232.
Tiffney, B.H., 1994. Re-evaluation of the age of the Brandon Lignite (Vermont, USA) based on plant megafossils. Rev. Palaeobot. Palynol. 82, 299–315.
Tiffney, B.H., Barghoorn, E.S., 1979. Flora of the Brandon Lignite. IV. Illiciaceae. Am. J. Bot. 66, 321–329.
Tiffney, B.H., Mancher, Fritsch, P.W., 2018. Two new species of *Symplocos* based on endocarps from the early Miocene Brandon Lignite of Vermont, USA. Acta Palaeobotanica 58, 185–198.
Traverse, A., 1994. Palynofloral geochronology of the Brandon Lignite of Vermont, USA. Rev. Palaeobot. Palynol. 82, 265–297.
Uhl, D., Herrmann, M., 2010. Palaeoclimate estimates for the late Oligocene taphoflora of Enspel (Westerwald, West Germany) based on palaeobotanical proxies. Palaeobiodivers. Palaeoenviron. 90, 39–47.
Utescher, T., Bruch, A.A., Erdei, B., François, L., Ivanov, D., Jacques, F.M.B., Kern, A.K., Liu, Y.-S., Mosbrugger, V., Spicer, R.A., 2014. The coexistence approach—Theoretical background and practical considerations of using plant fossils for climate quantification. Palaeogeogr. Palaeoclimatol. Palaeoecol. 410, 58–73.
Utescher, T., Dreist, A., Henrot, A.-J., Hickler, T., Liu, Y.-S., Mosbrugger, V., Portmann, F. T., Salzmann, U., 2017. Continental climate gradients in North America and Western Eurasia before and after the closure of the central American Seaway. Earth Planet. Sci. Lett. 472, 120–130.
Walker, J.D., Geissman, J.W., Bowring, S.A., Babcock, L.E., 2018. Geologic Time Scale v. 5.0. Geological Society of America.

Wallace, S.C., Wang, X., 2004. Two new carnivores from an unusual late Tertiary forest biota in eastern North America. Nature 431, 556–559.
Walsh, K.J.E., Camargo, S.J., Vecchi, G.A., Daloz, A.S., Elsner, J., Emanuel, K.A., Horn, M., Lim, Y.-K., Roberts, M., Patricola, C., Scoccimarro, E., Sobel, A.H., Strazzo, S., Villarini, G., Wehner, M., Zhao, M., Kossin, J.P., LaRow, T., Oouchi, K., Schubert, S., Wang, H., Bacmeister, J., Chang, P., Chauvin, F., Jablonowski, C., Kumar, A., Murakami, H., Ose, T., Reed, K.A., Saravanan, R., Yamada, Y., Zarzycki, C.M., Vidale, P.L., Jonas, J.A., Henderson, N., 2015. Hurricanes and climate: the U.S. CLIVAR working group on hurricanes. Bull. Am. Meteorol. Soc. 96, 997–1017.
Weems, R.E., Edwards, L.E., Landacre, B., 2017. Geology and biostratigraphy of the Potomac River cliffs at Stratford Hall, Westmoreland County, Virginia. In: Bailey, C. M., Jaye, S. (Eds.), From the Blue Ridge to the Beach: Geological Field Excursions across Virginia. Geological Society of America, McLean, Virginia, pp. 125–152.
West, C.K., Greenwood, D.R., Reichgelt, T., Lowe, A.J., Vachon, J.M., Basinger, J.F., 2020. Paleobotanical proxies for early Eocene climates and ecosystems in northern North America from middle to high latitudes. Clim. Past 16, 1387–1410.
West, C.K., Reichgelt, T., Basinger, J.F., 2021. The Ravenscrag Butte flora: Paleoclimate and paleoecology of an early Paleocene (Danian) warm-temperate deciduous forest near the vanishing inland Cannonball Seaway. Palaeogeogr. Palaeoclimatol. Palaeoecol. 576, 110488.
Westerhold, T., Marwan, N., Drury, A.J., Liebrand, D., Agnini, C., Anagnostou, E., Barnet, J.S.K., Bohaty, S.M., De Vleeschouwer, D., Florindo, F., Frederichs, T., Hodell, D.A., Holbourn, A.E., Kroon, D., Lauretano, V., Littler, K., Lourens, L.J., Lyle, M., Pälike, H., Röhl, U., Tian, J., Wilkens, R.H., Wilson, P.A., Zachos, J.C., 2020. An astronomically dated record of Earth's climate and its predictability over the last 66 million years. Science 369, 1383–1387.
Whittaker, R.H., 1962. Classification of natural communities. Bot. Rev. 28, 1–239.
Willard, D.A., Donders, T.H., Reichgelt, T., Greenwood, D.R., Sangiorgi, F., Peterse, F., Nierop, K.G.J., Frieling, J., Schouten, S., Sluijs, A., 2019. Arctic vegetation, temperature, and hydrology during early Eocene transient global warming events. Glob. Planet. Chang. 178, 139–152.
Williams-Linera, G., Toledo-Garibaldi, M., Gallardo Hernández, C., 2013. How heterogeneous are the cloud forest communities in the mountains of Central Veracruz, Mexico? Plant Ecol. 214, 685–701.
Wiser, S.K., De Cáceres, M., 2013. Updating vegetation classifications: an example with New Zealand's woody vegetation. J. Veg. Sci. 24, 80–93.
Witkowski, C.R., Weijers, J.W.H., Blais, B., Schouten, S., Sinninghe Damsté, J.S., 2018. Molecular fossils from phytoplankton reveal secular pCO_2 trend over the Phanerozoic. Sci. Adv. 4, 7.
Wolfe, J.A., Schorn, H.E., Forest, C.E., Molnar, P., 1997. Paleobotanical evidence for high altitudes in Nevada during the Miocene. Science 276, 1672–1675.
Wrenn, J.H., Elsik, W.C., McCulloh, R.P., 2003. Palynologic age determination of the Catahoula Formation, big Creek, Sicily Island, Louisiana. In: Gulf Coast Association of Geological Societies Transactions, 53, pp. 867–877.
Xie, Y., Wu, F., Fang, X., 2019. Middle Eocene East Asian monsoon prevalence over southern China: evidence from palynological records. Glob. Planet. Chang. 175, 13–26.
Yang, J., Spicer, R.A., Spicer, T.E.V., Arens, N.C., Jacques, F.M.B., Su, T., Kennedy, E.M., Herman, A.B., Steart, D.C., Srivastrava, G., Mehrotra, R.C., Valdes, P.J., Mehrotra, N. C., Zhou, Z.-K., Lai, J.-S., 2015. Leaf form–climate relationships on the global stage: an ensemble of characters. Glob. Ecol. Biogeogr. 24, 1113–1125.
Yao, Y.-F., Bera, S., Ferguson, D.K., Mosbrugger, V., Paudayal, K.N., Jin, J.-H., Li, C.-S., 2009. Reconstruction of paleovegetation and paleoclimate in the early and Middle Eocene, Hainan Island, China. Clim. Chang. 92, 169–189.
You, Y., Huber, M., Müller, R.D., Poulsen, C.J., Ribbe, J., 2009. Simulation of the Middle Miocene climate Optimum. Geophys. Res. Lett. 36. L04702.
Zobaa, M.K., Zavada, M.S., Whitelaw, M.J., Shunk, A.J., Oboh-Ikuenobe, F.E., 2011. Palynology and palynofacies analyses of the Gray Fossil Site, eastern Tennessee: their role in understanding the basin-fill history. Palaeogeogr. Palaeoclimatol. Palaeoecol. 308, 433–444.